MULTISCALE COMPUTATIONAL FRAMEWORK FOR FREE VIBRATION ANALYSIS OF BORON NITRIDE NANOTUBES AT FINITE TEMPERATURE

A THESIS

Submitted in partial fulfillment of the
requirements for the award of the degree
of
Master of Technology

by

ROHAN SHINDE

DEPARTMENT OF MECHANICAL ENGINEERING
INDIAN INSTITUTE OF TECHNOLOGY INDORE
JUNE 2025

CANDIDATE'S DECLARATION

I hereby certify that the work which is being presented in the thesis entitled **MULTISCALE COMPUTATIONAL FRAMEWORK OF FREE VIBRATION ANALYSIS OF BORON NITRIDE NANOTUBES AT FINITE TEMPERATURE** in the partial fulfillment of the requirements for the award of the degree of **MASTER OF TECHNOLOGY** and submitted in the **DEPARTMENT OF MECHANICAL ENGINEERING, Indian Institute of Technology Indore**, is an authentic record of my own work carried out during the time period from JULY 2023 to JUNE 2025 under the supervision of **Dr. Sandeep Singh**, Assistant Professor

The matter presented in this thesis has not been submitted by me for the award of any other degree of this or any other institute.

17/06/2025

ROHAN SHINDE
(M. TECH STUDENT)

This is to certify that the above statement made by the candidate is correct to the best of my/our knowledge.

(17/06/2025)

DR. SANDEEP SINGH
(THESIS SUPERVISOR)

ROHAN SHINDE has successfully given his/her M.Tech. Oral Examination held on **23 May 2023**.

(17/06/2025)

Signature(s) of Supervisor(s) of M.Tech. thesis
Date:

Convener, DPGC
Date: 19-06-2025

ACKNOWLEDGEMENTS

I am deeply thankful to my guide, **Dr Sandeep Singh**, for their continuous support, expert guidance, and encouragement throughout this research. Their insightful suggestions and constructive feedback were instrumental in shaping the direction and quality of this project.

I would also like to extend my heartfelt thanks to the Department of Mechanical Engineering, IIT Indore, for providing the resources, academic environment, and technical facilities that enabled me to carry out this work effectively.

My sincere appreciation goes to the faculty members and staff of the Mechanical System Design division, whose teachings and assistance contributed greatly to my understanding and growth during the M. Tech program.

I am also grateful to my fellow researchers and friends, especially Mr. Akash Raikwar (Ph.D. Scholar), for their cooperation, stimulating discussions, and moral support during challenging phases of the research.

A special word of thanks to my family, whose unwavering belief in me, constant encouragement, and emotional support kept me motivated throughout this journey.

Finally, I dedicate this work to all those who have directly or indirectly contributed to the successful completion of my M. Tech thesis.

(Rohan Shinde)

Abstract

This study proposes a multiscale computational approach that integrates finite temperature effects into the constitutive modeling for evaluating the thermal, mechanical, and free-vibration responses of single-walled boron nitride nanotubes (SWBNNTs). The framework is built upon a temperature-dependent quadratic Cauchy-Born rule, with atomic interactions described using the Tersoff-Brenner potential and various empirical parameter sets. The Helmholtz free energy of the representative unit cell is formulated as the sum of its interatomic potential energy and the thermal energy arising from atomic vibrations at finite temperatures. Stress, moment tensors, and the tangent stiffness matrix are derived by differentiating the Helmholtz free energy density with respect to strain and curvature. A finite element model in cylindrical coordinates is developed using a four-nodded membrane-consistent (4NMC) element, employing a smoothed interpolation technique in the circumferential direction to mitigate membrane locking. The influence of temperature on the natural frequencies of SWBNNTs is thoroughly analyzed, considering changes in nanotube length, radius, and various boundary conditions.

TABLE OF CONTENTS

LIST OF FIGURES

LIST OF TABLES

Chapter 1

Introduction

1. Introduction:

This chapter provides a comprehensive background on boron nitride nanotubes (BNNTs), emphasizing their unique structural features and outstanding physical properties. The need for accurate prediction of their behavior under thermal and mechanical environments is highlighted. The chapter introduces the simulation approaches used to study nanostructures, including continuum, atomistic, and multiscale methods, and establishes the motivation, significance, and objectives of the present work. It concludes with an overview of the thesis organization.

1.1 Overview:

Boron nitride nanotubes (BNNTs), particularly their single-walled form (SWBNNTs), have emerged as a subject of intense scientific interest due to their exceptional combination of structural and functional properties. Structurally analogous to carbon nanotubes but composed of alternating boron and nitrogen atoms, BNNTs possess a wide bandgap, high thermal conductivity, outstanding chemical stability, and remarkable mechanical strength. These features make them highly suitable for use in extreme environments and advanced nanotechnological applications.

Despite their potential, a comprehensive understanding of their behaviour under mechanical and thermal loading especially at the nanoscale remains a complex task. The discrete atomic structure of BNNTs means that classical continuum theories alone are insufficient to capture their size-dependent phenomena. Meanwhile, fully atomistic simulations, while accurate, are computationally demanding for large systems. This complexity

necessitates a modelling approach that balances accuracy with computational efficiency.

This research focuses on the development of a multiscale computational framework that bridges the gap between atomistic detail and continuum mechanics. The approach integrates temperature-dependent constitutive modelling with finite element analysis to investigate the thermomechanical and vibrational responses of SWBNNTs under various conditions. By incorporating the effects of finite temperature and large deformation, the study aims to provide a more realistic and predictive model for BNNT behaviour, thereby contributing to the design and reliability assessment of nanotube-based materials and devices.

1.2 Application of BNNTs:

Boron nitride nanotubes possess a unique combination of properties, such as high thermal conductivity, electrical insulation, chemical inertness, and mechanical resilience, making them ideal for a wide range of advanced applications.

 Aerospace Engineering: Used in high-strength, heat-resistant composite materials for structural components.

 Nanoelectronics: Serve as excellent electrical insulators in nanoscale electronic devices due to their wide bandgap and stability.

 Biomedical Field: Potential carriers for drug delivery systems and imaging agents due to their biocompatibility.

 Thermal Management: Employed in heat-dissipating materials for electronics and high-temperature applications.

 Nuclear and Space Technology: Suitable for use in extreme environments due to their resistance to radiation, oxidation, and high temperatures.

 Sensors and Actuators: Utilized in nanoscale mechanical systems due to their high stiffness and sensitivity to external stimuli.

1.3 Types of simulation approaches to study BNNTs:

Understanding the physical behavior of boron nitride nanotubes (BNNTs) requires simulation techniques that capture phenomena at different length and time scales. The choice of simulation approach depends on the level of detail required, computational resources, and the specific property or behavior being investigated. The primary categories of simulation methods used for studying BNNTs include continuum models, atomistic simulations, and multiscale frameworks. Each offers unique advantages and limitations.

1.3.1 Continuum Simulation

Continuum simulations treat materials as continuous media, ignoring the discrete nature of atoms. These methods are grounded in classical mechanics and are well-suited for modelling the mechanical behaviour of nanostructures at scales larger than individual atoms.

- **Principles**: The material is represented using field variables like stress, strain, and displacement. Governing equations derived from elasticity theory, thermos-elasticity, or shell theories are solved using numerical methods such as the Finite Element Method (FEM).
- **Application to BNNTs**: BNNTs, owing to their cylindrical geometry and high aspect ratio, are often modelled as nanoscale beams or shells using modified versions of classical shell theory. Continuum models are particularly useful for predicting deformation, buckling, vibration, and thermal expansion.
- **Limitations**: These models do not account for atomic-scale interactions and may not be accurate when nanoscale effects, such as surface energy or size-dependent mechanical properties, become significant.

1.3.2 Atomistic Simulation

Atomistic methods provide detailed insights by considering interactions between individual atoms. These simulations are essential for capturing quantum effects, chemical bonding, and thermal vibrations that are not addressed in continuum models. Two widely used atomistic techniques for BNNTs are Density Functional Theory (DFT) and Molecular Dynamics (MD).

a) Density Functional Theory (DFT)

- **Overview**: DFT is a quantum mechanical method used to investigate the electronic structure of materials. It solves the Schrödinger equation for electrons under the influence of nuclei using electron density as the primary variable.
- **Application to BNNTs**: DFT is used to calculate properties like band structure, electronic density of states, binding energy, and mechanical constants. It is especially valuable for studying electronic and optical properties of BNNTs or predicting their behaviour under external fields.
- **Strengths and Limitations**: DFT offers high accuracy but is computationally expensive, limiting its use to small systems or unit cells.

b) Molecular Dynamics (MD)

- **Overview**: MD simulates the time evolution of a system of atoms by numerically solving Newton's equations of motion. Interatomic forces are computed using empirical or semi-empirical potential functions.
- **Application to BNNTs**: MD allows the study of mechanical deformation, fracture behaviour, thermal conductivity, and vibrational

modes at finite temperatures. It captures dynamic phenomena like impact, heat transport, and structural transformations.

- **Strengths and Limitations**: MD handles large systems over nanosecond timescales, but its accuracy depends heavily on the choice of interatomic potential. It cannot capture quantum effects like electronic transitions.

1.3.3 Multiscale Simulation

Multiscale simulation bridges the gap between atomistic and continuum approaches by linking different models across spatial or temporal scales. This is particularly important for nanostructures like BNNTs, where localized atomic interactions influence overall mechanical behaviour.

- **Concept**: In a multiscale framework, the atomic-level information (e.g., from DFT or MD) is used to inform continuum models. This might involve computing material parameters like elastic constants or free energy from atomistic simulations and incorporating them into finite element models.
- **Techniques Used**:
    - **Cauchy-Born Rule**: Translates atomic displacements into continuum deformation fields.
    - **Coarse-Grained MD**: Reduces computational load by grouping atoms into larger units.
    - **Quasi continuum Method**: Couples regions of full atomistic resolution with continuum descriptions elsewhere.
- **Application to BNNTs**: Multiscale models can simulate large-scale behaviours such as buckling or wave propagation while still incorporating nanoscale material characteristics like temperature-dependent stiffness or anisotropic properties.

- **Advantages**: Provides a balance between accuracy and efficiency, making it suitable for analysing large structures with atomic-level precision in critical regions.

1.4 Significance and objective:

1.4.1 Significance of the Thesis

Single-walled boron nitride nanotubes (SWBNNTs) exhibit remarkable mechanical strength, thermal stability, and electrical insulation, positioning them as promising candidates for a variety of advanced engineering and technological applications. However, accurately predicting their behaviour under thermal and mechanical loading especially at the nanoscale remains a complex challenge. This thesis addresses that gap by developing a temperature-dependent multiscale modelling framework that links atomistic interactions to continuum mechanics. By capturing both thermal effects and mechanical responses, the research provides valuable insights into the real-world performance of SWBNNTs and contributes to the design of more reliable nanostructured materials.

1.4.2 Objectives of the Thesis

1. **To develop a multiscale computational model** that integrates finite temperature effects into the constitutive behaviour of SWBNNTs using a temperature-dependent Cauchy-Born rule.

2. **To accurately represent atomic interactions** through the Tersoff-Brenner potential using various empirical parameters, enabling precise evaluation of stress, moment tensors, and stiffness characteristics.

3. **To analyse the impact of thermal and geometric factors**—including temperature, length, and radius—on the natural frequencies and vibrational behaviour of SWBNNTs under different boundary conditions using a finite element framework.

1.5 Thesis outline:

The present thesis is systematically organized into six chapters to comprehensively address the thermal, mechanical, and vibrational behavior of single-walled boron nitride nanotubes (SWBNNTs) using a multiscale computational framework.

Chapter 1 introduces motivation, background, and research objectives, highlighting the need for advanced modeling techniques to study nanostructures.

Chapter 2 provides a detailed literature review, summarizing the existing experimental and theoretical approaches—namely atomistic, continuum, and multiscale simulations—used for analyzing the properties of BNNTs and related nanomaterials.

Chapter 3 develops a finite-temperature constitutive model based on the temperature-dependent quadratic-type Cauchy-Born rule, incorporating atomic interactions via the Tersoff-Brenner potential and deriving key thermomechanical expressions.

Chapter 4 formulates a finite element model capable of capturing large deformation and vibrational responses, employing a membrane-consistent element to improve numerical performance and account for temperature effects.

Chapter 5 presents and discusses simulation results, examining how geometric and thermal factors influence the constitutive behavior and vibrational characteristics of SWBNNTs, with comparisons to previous studies for validation.

Chapter 6 concludes the work by summarizing the key findings, outlining the contributions made, and proposing potential directions for future research to expand the applicability of the developed framework.

Chapter 2

Literature Review

2. Introduction:

An in-depth review of previous research on the modelling and analysis of carbon and boron-based nanostructures is presented in this chapter. Key contributions from experimental studies and simulation-based approaches are discussed. The chapter categorizes past work into atomistic simulations (e.g., DFT and MD), continuum mechanical models, and multiscale techniques, comparing their advantages, limitations, and suitability for predicting the thermomechanical response of BNNTs. Gaps in existing literature are identified to justify the scope of the current study.

Literature Review:

The journey to understand the mechanical behaviour of nanostructures began with experimental attempts, despite their complexity at the nanoscale. In a pioneering work, Chopra et al. (1997) used transmission electron microscopy (TEM) to measure the Young's modulus of individual multiwalled boron nitride nanotubes (BNNTs), reporting a value of approximately 1.22 ± 0.24 TPa. Around the same time, Krishnan et al. (1998) evaluated the stiffness of single-walled carbon nanotubes (SWCNTs) by observing their room-temperature vibrations through TEM, finding an average Young's modulus of 1.25 TPa. Although insightful, such experimental studies are extremely challenging due to the scale and geometry of the specimens, especially for prismatic, single-walled nanostructures.

To overcome these challenges, researchers began turning to theoretical and computational methods. These simulation approaches, particularly for BNNTs, can be broadly categorized into three major types: atomistic simulations, continuum modelling, and multiscale approaches that combine the two. As highlighted by Rafiee et al. (2013) in a comprehensive review of

carbon nanotube (CNT) modelling, each method offers distinct advantages depending on the problem's scale and required accuracy.

Atomistic simulations, such as Density Functional Theory (DFT) and Molecular Dynamics (MD), are widely used for their ability to capture interactions at the atomic level with high precision. DFT offers quantum mechanical insights into electronic structure and bonding, whereas MD simulations help understand time-dependent behaviour like thermal motion and mechanical response under various loading conditions. However, both methods come with a computational cost, limiting their practicality for large or complex systems.

In contrast, continuum mechanics models simplify the structure into beams, shells, or plates and apply classical elasticity theory. These models are computationally efficient and useful for analysing large-scale behaviour, but they lack atomic-scale resolution. Typically, the choice between beam or shell modelling depends on the nanotube's aspect ratio. For structures with a length-to-diameter ratio less than 35, shell models are used; for ratios above 35, beam models are preferred. Researchers like Yoon et al. (2003), Zhang et al. (2005), and Natsuki et al. (2010) have employed Euler-Bernoulli and Timoshenko beam theories to explore the vibrational behaviour of multiwalled CNTs. Similarly, Wang et al. (2006) incorporated non-local elasticity into beam theory to study single and double-walled CNTs.

Another interesting direction emerged with multiscale simulation techniques, which blend the accuracy of atomistic models with the efficiency of continuum mechanics. This hybrid approach enables capturing both the detailed atomic interactions and the overall structural response. For instance, Hernandez et al. (1995) applied tight-binding and first-principles methods to compute the mechanical properties and strain energy of single-walled nanotubes, finding that the Young’s modulus for BNNTs ranged from 0.837 to 0.912 TPa depending on diameter. Kudin et al. (2001) further explored the

properties of two-dimensional boron nitride and other nanomaterials using ab initio techniques.

In the realm of temperature-dependent behaviour, Han et al. (2014) examined how temperature and strain rate affect boron nitride nanosheets using MD simulations based on the AIREBO potential. Huang and Guo (2014) combined statistical mechanics and MD simulations to uncover how anharmonic vibrations contribute to the thermal expansion of monolayer graphene.

Multiscale modelling approaches continued to gain traction as they evolved. Researchers like Guo et al. (2006), Wang et al. (2006), and Huang et al. (2006) adopted various forms of the Cauchy-Born rule—such as higher-order and quadratic types—to bridge atomistic information with continuum deformation fields. Arroyo and Belytschko (2002, 2004) introduced the exponential Cauchy-Born rule to incorporate curvature effects in graphene and CNTs. Yan et al. (2015) implemented a higher-order Cauchy-Born rule, calibrated with Oh's empirical parameters, to predict BNNTs' elastic properties at zero temperature. More recent studies (e.g., Jiang et al., 2005; Guo et al., 2012; Raikwar and Singh, 2024) included temperature effects in multiscale frameworks using temperature-dependent versions of the Cauchy-Born rule.

The accuracy of interatomic potentials plays a critical role in MD simulations. Singh et al. (2020) evaluated eight different parameter sets for the Tersoff-Brenner potential for two-dimensional boron nitride structures and compared their results against theoretical predictions. Singh et al. (2021) further refined the attractive and repulsive parameters for nitride- and phosphide-based nanomaterials to improve predictions of elastic constants, nonlinear behaviour, and bending properties.

When applying continuum mechanics in vibrational studies, geometry heavily influences model selection. Structural studies by Kitipornchai et al. (2005), Rouhi et al. (2012), and Singh & Arghavan (2011) used Kirchhoff plate and space frame models to evaluate the vibrational response of graphene sheets.

Giannopoulos et al. (2016) utilized structural mechanics-based finite element modelling to investigate the resonance characteristics of SWBNNTs. Panchal et al. (2013) treated SWBNNTs as thin-walled cylindrical shells in FEM-based simulations to analyse their natural frequencies under different constraints.

Nonetheless, continuum methods fall short when capturing intricate interatomic forces, particularly in higher vibration modes. For instance, Wang et al. (2010) compared results from MD and beam models for CNTs, finding good agreement in lower modes, but divergence in higher ones—highlighting the value of Timoshenko beam theory for accuracy.

Further studies by Chaudhary et al. (2010) used molecular mechanics to explore the vibrational modes (radial, torsional, transverse) of zigzag and armchair BNNTs. Ansari et al. (2014, 2015) focused on how boundary conditions and nanotube length influence the transverse vibration of pure BNNTs and hybrid carbon-boron tubes. Darvishi et al. (2024) delved into coiled CNTs' free vibration response via MD.

To overcome the trade-off between accuracy and computational load, multiscale frameworks continue to be the method of choice. Sun et al. (2008a, 2008b) investigated buckling and vibration of CNTs using higher-order Cauchy-Born methods. Yan et al. (2013, 2014, 2017) extended these approaches using gradient theory and mesh-free methods to examine vibrational behaviour in carbon nano-cones and BNNTs with various chirality's and boundary conditions.

Building on this foundation, Singh and Patel (2018) explored the nonlinear static and dynamic responses of CNTs and graphene using multiscale FEM, introducing a 4-noded membrane-consistent element to mitigate membrane locking issues. Singh et al. (2023) expanded this to evaluate the large deformation behaviour of nitride and phosphide nanotubes at zero Kelvin. Most recently, Qi et al. (2023) combined higher-order Cauchy-Born rules with

a meshless Petrov-Galerkin scheme to analyse the buckling patterns and vibration characteristics of SWBNNTs under finite temperature conditions.

Chapter 3

Finite Temperature Constitutive Model

3. Introduction:

This chapter outlines the theoretical foundation for modeling thermomechanical behavior at the nanoscale. A temperature-dependent quadratic Cauchy-Born rule is used in combination with the Tersoff-Brenner potential to derive the constitutive relations. The Helmholtz free energy is formulated by accounting for interatomic potential energy and thermal vibrations based on the local harmonic approximation. Expressions for stress, moment tensors, and tangent stiffness matrices are derived, forming the core of the constitutive model for further finite element implementation.

3.1 Helmholtz free energy and local harmonic approximation:

Helmholtz free energy:

At finite temperature the Helmholtz free energy (A_H) is written as sum of total interatomic potential and kinetic energy due to thermal vibration of atoms, based on Quasi-harmonic approximation, the Helmholtz free energy of a system of size *N* is written as (Guo et al., 2012):

$$A_H = V_{tot} + K_B T \sum_{i=1}^{3} \sum_{\alpha=1}^{3} \ln\left[2\sinh\left(\frac{h_p \omega_{i\alpha}}{4\pi K_B T} \right) \right] \tag{1}$$

where V_{tot} is the total interatomic potential energy due to interatomic interaction, K_B is Boltzmann constant, h_p is planks constant, T is the absolute temperature , $\omega_{i\alpha}$ is the vibration frequency of atom i ($i = 1,2,3 \ldots N$) for α (α =1,2,3) degree of freedom and it can calculated from below characteristics equation:

$$\left| \frac{1}{m_1 m_2} \left(\frac{\partial^2 V_{tot}}{\partial \mathbf{x}_i \partial \mathbf{x}_i} \right)_{\mathbf{x}_i = \mathbf{x}_i(T)} - \mathbf{I}_{3N\times 3N} \omega_{i\alpha}^2 \right| = 0 \tag{2}$$

where m_1 is mass of boron atom and m_2 mass of nitrogen atom, $\mathbf{I}_{3N\times 3N}$ is identity matrix of $3N \times 3N$ size, solution of Eq. (2) requires computation of all eigen values associated with matrix of $3N\times 3N$ size, this is computationally expensive for large system, this can overcome through local harmonic approximation (LHA) (Guo et al., 2012)

Local Harmonic approximation (LHA):

In the representative unit cell as shown in the figure, the central atom i vibrates about their position and other atoms are kept fixed at their equilibrium position, based on this assumption Eq. (2) is modified and written as follows

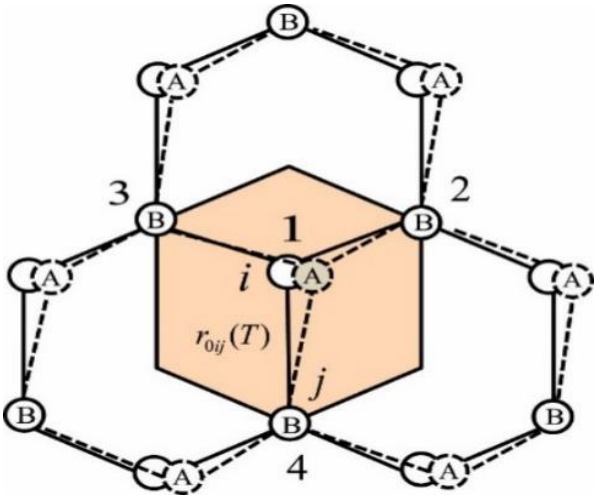

Figure 3.1. Unit cell with central vibrating atoms A and Surrounding atoms B

The modified form of Eq. (2) is written as:

$$\left| \frac{1}{m_1 m_2} \left(\frac{\partial^2 V_{tot}}{\partial \mathbf{x}_i \partial \mathbf{x}_i} \right)_{\mathbf{x}_i = \mathbf{x}_i(T)} - \mathbf{I}_{3\times 3}\omega_\alpha^2 \right| = 0 \qquad (3)$$

Where ω_α (α = 1,2,3) represents frequency of vibration of central atom (i =1), LHA employed for acceptable agreement between accuracy and computational cost. Based on LHA assumption Eq. (1) is modified as follows

$$A_H = V_{tot} + K_B T \sum_{\alpha=1}^{3} \ln\left[2\sinh\left(\frac{h_p \omega_\alpha}{4\pi K_B T} \right) \right] \tag{4}$$

3.2 Temperature related Cauchy-Born rule:

Cauchy-Born rule relates atomistic scale deformation with continuum scale deformation through deformation gradient: $\mathrm{r}_{ij}(T) = \mathbf{F}\mathbf{r}_{0ij}(T)$ (Jiang et al.,2005)

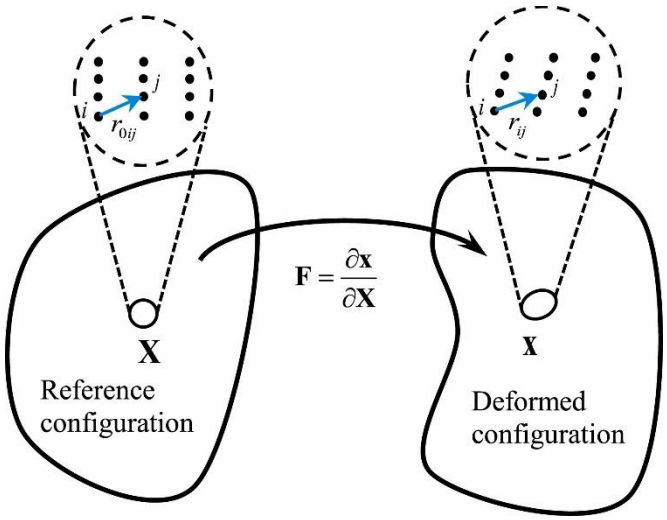

Figure 3.2. Deformation mapping from atomic level to the continuum level using Cauchy Born Rule

Quadratic type Cauchy-Born rule for non-centrosymmetric material including curvature effect (Huang et al., 2006), second term in deformed bond length equation accounts curvature effect

$$r_{ij} = r_0(T)\sqrt{(\mathbf{n}_{0ij}+\boldsymbol{\eta})\cdot(\mathbf{I}+2\mathbf{E})(\mathbf{n}_{0ij}+\boldsymbol{\eta}) - \frac{(r_0(T))^2}{12}\left[(\mathbf{n}_{0ij}+\boldsymbol{\eta})\cdot\mathbf{K}(\mathbf{n}_{0ij}+\boldsymbol{\eta})\right]^2} \tag{5}$$

3.3 Constitutive Modelling based on Finite Temperature:

Strain energy density based on Helmholtz free energy can be written as follows. (Jiang et al., 2005) where Ω is area of the unit cell $\Omega = \frac{3\sqrt{3}}{2}\left(r_0(T)\right)^2$

$$W(\mathbf{E},\mathbf{K},T) = \frac{1}{\Omega}\left\{V_{tot} + K_B T \sum_{\alpha=1}^{3} \ln\left[2\sinh\left(\frac{h_p \omega_\alpha}{4\pi K_B T}\right)\right]\right\} \tag{6a}$$

$$W = W\left(\mathbf{E},\mathbf{K},\boldsymbol{\eta}(\mathbf{E},\mathbf{K}),T\right) \tag{6b}$$

The second Piola-Kirchhoff stress tensor **S** and moment tensor **M** are obtained by differentiating the strain energy with respect to **E** and **K**, respectively

$$\mathbf{S} = \frac{\partial W}{\partial \mathbf{E}} = \frac{1}{\Omega}\left[\frac{\partial V_{tot}}{\partial \mathbf{E}} + \frac{h_p}{4\pi}\sum_{\alpha=1}^{3}\coth\left(\frac{h_p \omega_\alpha}{4\pi K_B T}\frac{\partial \omega_\alpha}{\partial \mathbf{E}}\right)\right] \tag{7a}$$

$$\mathbf{M} = \frac{\partial W}{\partial \mathbf{K}} = \frac{1}{\Omega}\left[\frac{\partial V_{tot}}{\partial \mathbf{K}} + \frac{h_p}{4\pi}\sum_{\alpha=1}^{3}\coth\left(\frac{h_p \omega_\alpha}{4\pi K_B T}\frac{\partial \omega_\alpha}{\partial \mathbf{K}}\right)\right] \tag{7b}$$

The incremental stress resultant tensor $\Delta\mathbf{S}$ and incremental moment resultant tensor $\Delta\mathbf{M}$ are related to the incremental strain tensor $\Delta\mathbf{E}$ and incremental curvature tensor $\Delta\mathbf{K}$ as :

$$\begin{Bmatrix}\Delta\mathbf{S}\\ \Delta\mathbf{M}\end{Bmatrix} = \begin{bmatrix}\mathbf{A} & \mathbf{B}\\ \mathbf{B}^T & \mathbf{D}\end{bmatrix}\begin{Bmatrix}\Delta\mathbf{E}\\ \Delta\mathbf{K}\end{Bmatrix}, \text{ and denoting } \bar{\mathbf{D}} = \begin{bmatrix}\mathbf{A} & \mathbf{B}\\ \mathbf{B}^T & \mathbf{D}\end{bmatrix} \tag{8}$$

The tangent stiffness coefficient (**A** , **B** and **D**) matrices are obtained through the double derivative of strain energy (W) with respect to **E** and **K**, respectively (Singh and Patel, 2015)

$$\mathbf{A} = \frac{D}{D\mathbf{E}}\left(\frac{\partial W}{\partial \mathbf{E}}\right) = \frac{\partial^2 W}{\partial \mathbf{E}\partial \mathbf{E}} - \left(\frac{\partial^2 W}{\partial \mathbf{E}\partial \boldsymbol{\eta}}\right)\left(\frac{\partial^2 W}{\partial \boldsymbol{\eta}\partial \boldsymbol{\eta}}\right)^{-1}\left(\frac{\partial^2 W}{\partial \boldsymbol{\eta}\partial \mathbf{E}}\right) \tag{9a}$$

$$\mathbf{B} = \frac{D}{D\mathbf{K}}\left(\frac{\partial W}{\partial \mathbf{E}}\right) = \frac{\partial^2 W}{\partial \mathbf{E}\partial \mathbf{K}} - \left(\frac{\partial^2 W}{\partial \mathbf{E}\partial \boldsymbol{\eta}}\right)\left(\frac{\partial^2 W}{\partial \boldsymbol{\eta}\partial \boldsymbol{\eta}}\right)^{-1}\left(\frac{\partial^2 W}{\partial \boldsymbol{\eta}\partial \mathbf{K}}\right) \tag{9b}$$

$$\mathbf{D} = \frac{D}{D\mathbf{K}}\left(\frac{\partial W}{\partial \mathbf{K}}\right) = \frac{\partial^2 W}{\partial \mathbf{K}\partial \mathbf{K}} - \left(\frac{\partial^2 W}{\partial \mathbf{K}\partial \boldsymbol{\eta}}\right)\left(\frac{\partial^2 W}{\partial \boldsymbol{\eta}\partial \boldsymbol{\eta}}\right)^{-1}\left(\frac{\partial^2 W}{\partial \boldsymbol{\eta}\partial \mathbf{K}}\right) \tag{9c}$$

The matrix **A** represents the tangent extensional stiffness, **B** denotes the bending-stretching coupling stiffness, and **D** stands for the tangent bending stiffness. Both the extensional stiffness matrix (**A**) and the bending stiffness matrix (**D**) are symmetric with respect to their main diagonals, reflecting the physical nature of pure stretching and bending responses. In contrast, the coupling stiffness matrix (**B**) is generally asymmetric, as it arises from mixed partial derivatives of the strain energy function with respect to strain and curvature, capturing the interaction between stretching and bending deformations.

So, to find residual strain and shift vectors we minimize strain energy density function with respect to residual strain and shift vectors.

$$W = W\left(\eta_1, \eta_2, E_{11}, E_{22}, E_{12}\right) \tag{10}$$

Solving the five nonlinear equations given below simultaneously by using newton- Raphson method until convergence criteria satisfied, res (5,1) represents five nonlinear equations and Tanmat (5,5) represents Jacobian or derivatives of 5 nonlinear equations. We have developed in-house FORTRAN subroutine to solve these five non-linear equations simultaneously.

$$\text{res}(5,1) = \begin{bmatrix} \frac{\partial W}{\partial \eta_1} \\ \frac{\partial W}{\partial \eta_2} \\ \frac{\partial W}{\partial E_{11}} \\ \frac{\partial W}{\partial E_{22}} \\ \frac{\partial W}{\partial E_{12}} \end{bmatrix} \text{Tanmat}(5\times 5) = \begin{bmatrix} \frac{\partial^2 W}{\partial \eta_1 \partial \eta_1} & \frac{\partial^2 W}{\partial \eta_1 \partial \eta_2} & \frac{\partial^2 W}{\partial E_{11} \partial \eta_1} & \frac{\partial^2 W}{\partial E_{22} \partial \eta_1} & \frac{\partial^2 W}{\partial E_{12} \partial \eta_1} \\ \frac{\partial^2 W}{\partial \eta_1 \partial \eta_2} & \frac{\partial^2 W}{\partial \eta_1 \partial \eta_1} & \frac{\partial^2 W}{\partial E_{11} \partial \eta_2} & \frac{\partial^2 W}{\partial E_{22} \partial \eta_1} & \frac{\partial^2 W}{\partial E_{12} \partial \eta_1} \\ \frac{\partial^2 W}{\partial E_{11} \partial \eta_1} & \frac{\partial^2 W}{\partial E_{11} \partial \eta_2} & \frac{\partial^2 W}{\partial E_{11} \partial E_{11}} & \frac{\partial^2 W}{\partial E_{11} \partial E_{22}} & \frac{\partial^2 W}{\partial E_{11} \partial E_{12}} \\ \frac{\partial^2 W}{\partial E_{22} \partial \eta_1} & \frac{\partial^2 W}{\partial E_{22} \partial \eta_2} & \frac{\partial^2 W}{\partial E_{22} \partial E_{11}} & \frac{\partial^2 W}{\partial E_{22} \partial E_{22}} & \frac{\partial^2 W}{\partial E_{22} \partial E_{12}} \\ \frac{\partial^2 W}{\partial E_{12} \partial \eta_1} & \frac{\partial^2 W}{\partial E_{12} \partial \eta_2} & \frac{\partial^2 W}{\partial E_{12} \partial E_{11}} & \frac{\partial^2 W}{\partial E_{12} \partial E_{22}} & \frac{\partial^2 W}{\partial E_{12} \partial E_{12}} \end{bmatrix} \tag{11a}$$

BNNT tries to relax to their equilibrium state, that's why it is essential to solve these five non-linear equations to find out residual shift vector and strain

Solution using newton-Raphson method:

$$\left[\text{Tanmat}\right]_{5\times5}^{-1}\times\left[\text{res}\right]_{5\times1}=\left[\text{Incre sol}\right]_{5\times1} \tag{11b}$$

Solution after satisfying convergence criteria:

$$\text{Sol}(5,1)=\begin{bmatrix}\eta_1\\ \eta_2\\ E_{11}\\ E_{22}\\ E_{12}\end{bmatrix} \tag{12}$$

The convergence criteria ensure that the computed residual strain and shift vectors correspond to a physically meaningful relaxed configuration of the BNNT structure.

$\lambda_1(T)$ and $\lambda_2(T)$ also represents the stretches in axial and circumferential direction and can be calculated from residual strain, curvature (K_{11}) can a be calculated from residual strain.

$$\begin{aligned}\lambda_1&=\sqrt{1+2E_{11}}\\ \lambda_2&=\sqrt{1+2E_{22}}\\ K_{11}&=\frac{1+2E_{11}}{R}\end{aligned} \tag{13}$$

By putting values of residual shift vector, strains and curvature in equation (7), the tangent stiffness matrix at reference configuration is calculated

$$\begin{Bmatrix} \Delta S_{11} \\ \Delta S_{22} \\ \Delta S_{12} \\ \Delta M_{11} \\ \Delta M_{22} \\ \Delta M_{12} \end{Bmatrix} = \begin{bmatrix} A_{11} & A_{12} & A_{13} & B_{11} & B_{12} & B_{13} \\ A_{21} & A_{22} & A_{23} & B_{21} & B_{22} & B_{23} \\ A_{31} & A_{32} & A_{33} & B_{31} & B_{32} & B_{33} \\ B_{11} & B_{21} & B_{31} & D_{11} & D_{12} & D_{13} \\ B_{12} & B_{22} & B_{32} & D_{21} & D_{22} & D_{23} \\ B_{13} & B_{23} & B_{33} & D_{31} & D_{32} & D_{33} \end{bmatrix} \begin{Bmatrix} \Delta E_{11} \\ \Delta E_{22} \\ 2\Delta E_{12} \\ \Delta K_{11} \\ \Delta K_{22} \\ 2\Delta K_{12} \end{Bmatrix} \tag{14}$$

Youngs modulus, Poisson ratio and shear modulus can be obtained from components of extensional stiffness coefficient matrix A as:

$$E_1 = \frac{1}{h}\left(A_{11} - \frac{A_{12}^2}{A_{22}} \right) \tag{15a}$$

$$\upsilon_{12} = \frac{A_{12}}{A_{11}} \tag{15b}$$

$$G_{12} = \frac{A_{22} - A_{12}}{2h} \tag{15c}$$

Chapter 4

Finite Element Formulation

4. Introduction:

Building on the constitutive framework, this chapter focuses on the development of a nonlinear finite element model to capture large deformation behavior and vibrational characteristics of SWBNNTs. A four-nodded membrane-consistent shell element is used to accurately represent the cylindrical geometry of nanotubes and to overcome numerical issues like membrane locking. The finite element formulation is presented in cylindrical coordinates, and the model is used to perform free vibration analysis under various thermal and geometric conditions.

4.1 Finite Element Formulation for free vibration analysis:

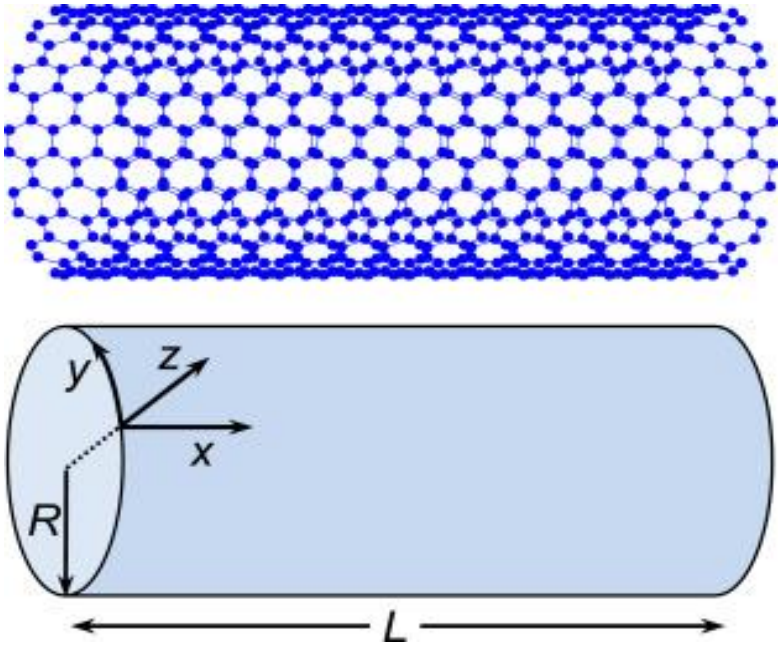

Figure 4.1. Schematic diagram of armchair SWBNNT and co-ordinate system used for multiscale-shell model

For thin cylindrical shells strain-displacement and curvature-displacement relations are expressed as

$$E_{xx} = \frac{\partial u}{\partial x} + \frac{1}{2}\left(\left(\frac{\partial w}{\partial x}\right)^2 + \left(\frac{\partial u}{\partial x}\right)^2 + \left(\frac{\partial v}{\partial x}\right)^2\right)$$

$$E_{yy} = \frac{\partial v}{\partial y} + \frac{w}{R} + \frac{1}{2}\left(\left(\frac{\partial w}{\partial y} - \frac{v}{R}\right)^2 + \left(\frac{\partial v}{\partial y} + \frac{w}{R}\right)^2 + \left(\frac{\partial u}{\partial y}\right)^2\right) \tag{16a}$$

$$E_{xy} = \frac{1}{2}\left(\frac{\partial u}{\partial y} + \frac{\partial v}{\partial x} + \left(\frac{\partial w}{\partial y} - \frac{v}{R}\right)\frac{\partial w}{\partial x} + \left(\frac{\partial v}{\partial y} + \frac{w}{R}\right)\frac{\partial v}{\partial x} + \frac{\partial u}{\partial y}\frac{\partial u}{\partial x}\right)$$

$$K_{xx} = \frac{\partial^2 w}{\partial x^2}; \quad K_{yy} = \frac{\partial^2 w}{\partial y^2} - \frac{\partial v}{R\partial y}; \quad K_{xy} = \frac{\partial^2 w}{\partial x \partial y} - \frac{\partial v}{2R\partial x} \tag{16b}$$

Hamilton principle is used to obtain equation of motion for the system

$$\int_{t_1}^{t_2} \left(\delta T - \delta W + \delta L\right) dt = 0 \tag{17}$$

The first variation of kinetic energy, strain energy and virtual work due to transverse load

$$\delta T = \int_{\Gamma_0} \rho \delta \dot{\mathbf{d}}^T \dot{\mathbf{d}}\, d\Gamma_0; \;\; \delta W = \int_{\Gamma_0} \left(\delta \mathbf{E}^T \mathbf{S} + \delta \mathbf{K}^T \mathbf{M}\right) d\Gamma_0; \;\; \delta L = \int_{\Gamma_0} \delta w^T Q\, d\Gamma_0 \tag{18}$$

By putting first variation of kinetic energy, strain energy and virtual work in equation and by invoking the arbitrariness of $\delta\mathbf{d}$ the equation can be expressed as

$$-\int_{\Gamma_0} \rho \delta \mathbf{d}^T \ddot{\mathbf{d}}\, d\Gamma_0 - \int_{\Gamma_0} \left(\delta \mathbf{E}^T \mathbf{S} + \delta \mathbf{K}^T \mathbf{M}\right) d\Gamma_0 + \int_{\Gamma_0} \delta w^T Q\, d\Gamma_0 = 0 \tag{19}$$

For interpolation of in-plane displacements *u* and *v* lagrangian interpolation function is used and for interpolation of transverse displacement *w* bi-cubic Hermite interpolation function is used

$$u = \sum_i N_i u_i; \; v = \sum_i N_i v_i; \; w = \sum_i H_i d_{wi} \tag{20}$$

$$E_{xx}^{l}=\frac{\partial u}{\partial x}=\sum_i \frac{\partial N_i}{\partial x}u_i$$

$$E_{xx}^{nl}=\frac{1}{2}\left(\left(\frac{\partial w}{\partial x}\right)^2+\left(\frac{\partial u}{\partial x}\right)^2+\left(\frac{\partial v}{\partial x}\right)^2\right)=\frac{1}{2}\left(\left(\sum_i \frac{\partial H_i}{\partial x}d_{wi}\right)^2+\left(\sum_i \frac{\partial N_i}{\partial x}u_i\right)^2+\left(\sum_i \frac{\partial N_i}{\partial x}v_i\right)^2\right)$$

$$E_{yy}^{l}=\frac{\partial v}{\partial y}+\frac{w}{R}=\sum_i \frac{\partial N_i}{\partial y}y_i+\sum_i H_i\frac{d_{wi}}{R}$$

$$E_{yy}^{nl}=\frac{1}{2}\begin{pmatrix}\left(\frac{\partial w}{\partial y}-\frac{v}{R}\right)^2+\\ \left(\frac{\partial v}{\partial y}+\frac{w}{R}\right)^2+\\ \left(\frac{\partial u}{\partial y}\right)^2\end{pmatrix}=\frac{1}{2}\begin{pmatrix}\left(\sum_i \frac{\partial H_i}{\partial y}d_{wi}-\sum_i N_i\frac{v_i}{R}\right)^2+\\ \left(\sum_i \frac{\partial N_i}{\partial y}v_i+\sum_i \frac{H_i}{R}d_{wi}\right)^2+\\ \left(\sum_i \frac{\partial N_i}{\partial y}u_i\right)^2\end{pmatrix}$$

$$2E_{xy}^{l}=\frac{\partial u}{\partial y}+\frac{\partial v}{\partial x}=\sum_i \frac{\partial N_i}{\partial y}u_i+\sum_i \frac{\partial N_i}{\partial x}v_i$$

$$2E_{xy}^{nl}=\begin{pmatrix}\left(\frac{\partial w}{\partial y}-\frac{v}{R}\right)\frac{\partial w}{\partial x}+\\ \left(\frac{\partial v}{\partial y}+\frac{w}{R}\right)\frac{\partial v}{\partial x}+\\ \frac{\partial u}{\partial y}\frac{\partial u}{\partial x}\end{pmatrix}=\begin{pmatrix}\left(\sum_i \frac{\partial H_i}{\partial y}d_{wi}-\sum_i N_i\frac{v_i}{R}\right)\left(\sum_i \frac{\partial H_i}{\partial x}d_{wi}\right)+\\ \left(\sum_i \frac{\partial N_i}{\partial y}v_i+\sum_i \frac{H_i}{R}d_{wi}\right)\left(\sum_i \frac{\partial N_i}{\partial x}v_i\right)+\\ \left(\sum_i \frac{\partial N_i}{\partial y}u_i\right)\left(\sum_i \frac{\partial N_i}{\partial x}u_i\right)\end{pmatrix} \quad (21)$$

$$K_{xx}=\frac{\partial^2 w}{\partial x^2}=\sum_i \frac{\partial^2 H_i}{\partial x^2}d_{wi}$$

$$K_{yy}=\frac{\partial^2 w}{\partial y^2}-\frac{\partial v}{R\partial y}=\sum_i \frac{\partial^2 H_i}{\partial y^2}d_{wi}-\frac{1}{R}\sum_i \frac{\partial N_i}{\partial y}v_i$$

$$2K_{xy}=2\frac{\partial^2 w}{\partial x\partial y}-\frac{\partial v}{R\partial x}=2\sum_i \frac{\partial^2 H_i}{\partial x\partial y}d_{wi}-\frac{1}{R}\sum_i \frac{\partial N_i}{\partial x}v_i$$

$$\mathbf{d}_w=\left[w_1,\left(\frac{\partial w}{\partial x}\right)_1,\left(\frac{\partial w}{\partial y}\right)_1,\left(\frac{\partial^2 w}{\partial x\partial y}\right)_1,w_2,.....,w_4,\left(\frac{\partial w}{\partial x}\right)_4,\left(\frac{\partial w}{\partial y}\right)_4,\left(\frac{\partial^2 w}{\partial x\partial y}\right)_4\right] \quad (22)$$

The membrane locking coming from interpolation of circumferential strain, the first term of linear part of circumferential strain is constant and second term is cubic in natural co-ordinates, this inconsistency leads to membrane locking.

$$E_{yy}^{l} = \frac{\partial v}{\partial y} + \frac{w}{R} = \sum_i \frac{\partial N_i}{\partial y} v_i + \sum_i H_i \frac{d_{wi}}{R} \tag{23}$$

The smoothed interpolation functions H_i for w in linear part of circumferential strain are derived through least square procedure are expressed as follows

$$\int_{-1}^{1}\int_{-1}^{1} \left(H_i - \left(a + b\xi\right)\right)^2 d\xi d\eta \tag{24}$$

By minimizing this equation with respect to a and b we obtain the following expression

$$\bar{H}_1 = \frac{1}{4} - \frac{3}{10}\xi; \quad \bar{H}_2 = \left(\frac{1}{12} - \frac{1}{20}\xi\right)\frac{l_x}{2}$$
$$\bar{H}_3 = \left(\frac{1}{12} - \frac{1}{10}\xi\right)\frac{l_y}{2}; \quad \bar{H}_4 = \left(\frac{1}{36} - \frac{1}{60}\xi\right)\frac{l_x l_y}{4}$$
$$H_5 = \frac{1}{4} + \frac{3}{10}\xi; \quad \bar{H}_6 = \left(-\frac{1}{12} - \frac{1}{20}\xi\right)\frac{l_x}{2}$$
$$\bar{H}_7 = \left(\frac{1}{12} + \frac{1}{10}\xi\right)\frac{l_y}{2}; \quad \bar{H}_8 = \left(-\frac{1}{36} - \frac{1}{60}\xi\right)\frac{l_x l_y}{4}$$
$$\bar{H}_9 = \frac{1}{4} + \frac{3}{10}\xi; \quad \bar{H}_{10} = \left(-\frac{1}{12} - \frac{1}{20}\xi\right)\frac{l_x}{2}$$
$$\bar{H}_{11} = \left(-\frac{1}{12} - \frac{1}{10}\xi\right)\frac{l_y}{2}; \quad \bar{H}_{12} = \left(\frac{1}{36} + \frac{1}{60}\xi\right)\frac{l_x l_y}{4}$$
$$\bar{H}_{13} = \frac{1}{4} - \frac{3}{10}\xi; \quad \bar{H}_{14} = \left(\frac{1}{12} - \frac{1}{20}\xi\right)\frac{l_x}{2}$$
$$\bar{H}_{15} = \left(-\frac{1}{12} + \frac{1}{10}\xi\right)\frac{l_y}{2}; \quad \bar{H}_{16} = \left(-\frac{1}{36} + \frac{1}{60}\xi\right)\frac{l_x l_y}{4} \tag{25}$$

By putting the values of nodal variables and interpolation function in equation

$$-\int_{\Gamma_e} \delta\mathbf{d}_e^T \rho \mathbf{U}^T \mathbf{U} \ddot{\mathbf{d}}_e d\Gamma_e - \int_{\Gamma_e} \delta\mathbf{d}_e^T \left[\mathbf{B} + \mathbf{B}_{NL}\right]^T \begin{bmatrix}\mathbf{S}\\ \mathbf{M}\end{bmatrix} d\Gamma_e + \int_{\Gamma_e} \delta\mathbf{d}_e^T \mathbf{H}^T Q d\Gamma_e + \delta\mathbf{d}_e^T \mathbf{F}_e^b = 0$$

(26)

Where **B** is linear strain/curvature displacement matrix, $\mathbf{B}_{NL}$ is non-linear strain curvature displacement matrix, **U** is interpolation matrix for displacement field, **H** is transverse displacement interpolation vector, $\mathbf{K}_{Te}$ is the elemental tangent stiffness matrix, $\mathbf{K}_{Ge}$ is elemental geometric stiffness

matrix, $\mathbf{F}_e$ is elemental external load vector, $\mathbf{F}_e{}^b$ is force vector due stress/moment resultants along boundary of element.

The elemental equation of motion for BNNT can be written as:

$$\bar{\mathbf{M}}_e\ddot{\mathbf{d}}_e + \int_{\Gamma_e} \delta\mathbf{d}_e^T \left[\mathbf{B}+\mathbf{B}_{NL}\right]^T \begin{bmatrix}\mathbf{S}\\ \mathbf{M}\end{bmatrix} d\Gamma_e = \mathbf{F}_e + \mathbf{F}_e^b \tag{27}$$

The linearized form of equation using Taylor series expansion is expressed as:

$$\bar{\mathbf{M}}_e\ddot{\mathbf{d}}_e + \mathbf{K}_{Te}\,|_n\,\Delta\mathbf{d}_e^{n+1} + \mathbf{F}_{ine}\,|_n = \mathbf{F}_e + \mathbf{F}_e^b \tag{28}$$

$$\mathbf{K}_{Te} = \int_{\Gamma_e} \left[\mathbf{B}+\mathbf{B}_{NL}\right]^T \left[\bar{\mathbf{D}}\right]\left[\mathbf{B}+\mathbf{B}_{NL}\right] d\Gamma_e + \mathbf{K}_{Ge}$$

$$\mathbf{K}_{Ge} = \int_{\Gamma_e} \bar{\mathbf{B}}^T\bar{\mathbf{S}}\bar{\mathbf{B}}\,d\Gamma_e,\quad \mathbf{F}_{ine} = \int_{\Gamma_e} \left[\mathbf{B}+\mathbf{B}_{NL}\right]^T \begin{bmatrix}\mathbf{S}\\ \mathbf{M}\end{bmatrix} d\Gamma_e,\quad \mathbf{F}_e = \int_{\Gamma_e} \mathbf{H}^T Q\,d\Gamma_e, \tag{29}$$

The components of matrix $\bar{\mathbf{S}}$ is expressed as:

$$\bar{\mathbf{S}} = \begin{bmatrix} S_{xx} & S_{xy} & 0 & 0 & 0 & 0\\ S_{xy} & S_{yy} & 0 & 0 & 0 & 0\\ 0 & 0 & S_{xx} & S_{xy} & 0 & 0\\ 0 & 0 & S_{xy} & S_{yy} & 0 & 0\\ 0 & 0 & 0 & 0 & S_{xx} & S_{xy}\\ 0 & 0 & 0 & 0 & S_{xy} & S_{yy} \end{bmatrix} \tag{30}$$

By assembling the element level equation of motion, the global equation of motion is expressed as:

$$\bar{\mathbf{M}}\ddot{\mathbf{d}} + \mathbf{K}_T\Delta\mathbf{d} + \mathbf{F}_{in} = \mathbf{F} \tag{31}$$

Eigen value problem for free vibration analysis is expressed as:

$$\left[\mathbf{K}_L - \omega_{ni}^2\bar{\mathbf{M}}\right]\{\mathbf{d}_i\} = 0 \tag{32}$$

Boundary conditions for the analysis:

$$\begin{aligned} &\text{Clamped - Clamped (C - C)}: u = v = w = \frac{\partial w}{\partial x} = \frac{\partial w}{\partial y} = \frac{\partial^2 w}{\partial x\partial y} = 0\\ &\text{Simply supported (S - S)}: u = v = w = \frac{\partial w}{\partial y} = M_{xx} = 0 \end{aligned} \tag{33}$$

Table 4.1. Empirical parameters are used in attractive and repulsive terms in Tersoff-Brenner potential

Parameters	Singh	Los	Oh
D_0 (eV)	5.99015	6.36	6.36
β (1/nm)	20.52903	19.932	22
S	1.13625	1.0953	1.0769
n	1	0.6577	1
a_0 ($\times 10^{-4}$)	2.0813	27.024851	2.0813
c_0	330	306.5866	330
d_0	3.5	10	3.5
h	-1	-0.7218	-1
r_e (nm)	0.1352	0.13254	0.133
δ	1/2n	1/2n	0.3820
r_0 (nm) (T = 300 K)	0.144872258	0.14456496	0.14489399

4.2 Modal mass participation:

Modal mass is the effective mass associated with a particular mode shape of a vibrating structure. It quantifies how much of the systems mass participate in a given mode of vibration. Each structure has multiple natural modes of vibration. In each mode, different parts of the structure move differently, modal mass tells us how much of the total mass participates in specific mode. It is important in deciding how many modes shapes are to be included in our analysis, modal mass participation tells how much of the total system mass is captured by each mode

Cumulative modal mass participation includes enough modes until 80-85% of the total mass captured

For a mode shape vector φ_i, the modal mass M_i is computed as:

$$M_i = \phi_i^T M \phi_i \tag{34}$$

Where,

φ_i : mode shape vector for mode *i*

M: mass matrix of the system

M_i : Modal mass of mode *i*

By normalizing modal mass of mode *i* by total mass of the system modal mass fraction is computed as:

$$\text{Modal mass percentage} = \frac{M_i}{M_{total}} \times 100 \tag{35}$$

Table 4.2. Modal mass participation for BNNT (8,8) with length 6nm and for clamped-clamped boundary condition at 900 K temperature.

Number of modes	Modal mass participation (%)
Mode 1	35.3060
Mode 2	14.8625
Mode 3	10.1434
Mode 4	7.4543
Mode 5	7.0876
Mode 6	5.7688
Cumulative modal mass participation	80.6226

In the current analysis, it was observed that the first six modes together account for a cumulative modal mass participation of approximately 80.62%. This indicates that the dominant dynamic behavior of the structure is sufficiently represented within these six modes. Extending the extraction to ten modes increases the cumulative participation to around 90.56%, but it was noted that individual contributions beyond the sixth mode fall below 5%, which means they have relatively minor influence. Hence, for the purpose of efficiency and relevance, only the first six modes are considered in this study.

This selection not only reduces computational effort but also ensures that the most dynamically significant modes are accurately included in the finite element analysis, leading to meaningful results in vibration characterization

Chapter 5

Results and Discussion

5. Introduction:

This chapter presents and interprets the results obtained from the proposed multiscale model. Thermal properties such as specific heat and thermal expansion, and mechanical properties including Young's modulus, Poisson's ratio, and shear modulus are evaluated. Vibration analysis is carried out to assess the influence of temperature, radius, and length on the natural frequencies of SWBNNTs. Mode shapes are analyzed at different temperatures, and modal mass participation is used to determine the significance of each vibrational mode. Comparisons with available DFT and molecular simulation data validate the accuracy of the model.

5.1 Multiscale constitutive modelling results:

5.1.1 Thermal properties of BNNTs:

(a) Specific heat:

In this study, the specific heat of single-walled boron nitride nanotubes (SWBNNTs) was evaluated over a range of temperatures using a finite temperature-based multiscale framework. The specific heat represents the material's capacity to absorb thermal energy, and its variation with temperature provides key insights into the thermal behavior of BNNTs at the atomic scale. based on local harmonic approximation (LHA) specific heat of BNNT is expressed by following expression (Guo et al., 2012)

$$C_V = \frac{h^2}{4k_B T^2 \Omega_1} \sum_{k=1}^{3} \frac{\omega_k^2}{\sinh^2\left[\frac{h\omega_k}{2k_B T}\right]} \tag{35}$$

- The results show that the specific heat increases rapidly at lower temperatures and then gradually approaches a saturation point as temperature continues to rise.
- This trend is typical for crystalline solids and reflects the anharmonic nature of atomic vibrations. At low temperatures, the vibrational modes are not fully activated, so specific heat rises sharply. As temperature increases, more modes become active until most are excited, leading to a gradual levelling off.
- At high temperatures (beyond 1500 K), the specific heat tends to reach a nearly constant value, in agreement with the classical Dulong–Petit law. This indicates that all degrees of freedom are thermally activated.

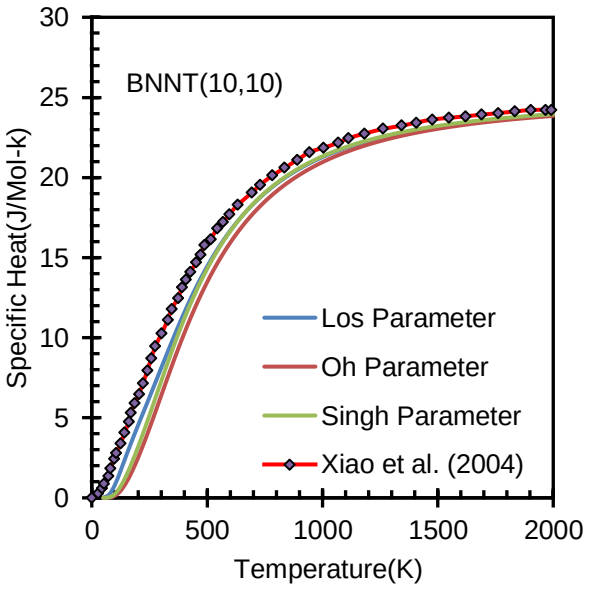

Figure 5.1. Specific heat variation of BNNT with temperature by using different potential parameters and compared with DFT result of (Xiao et al.,2004)

- The computed results using different empirical potential parameter sets (such as Los, Oh, and Singh) all show the same overall behavior. Minor variations exist in absolute values, which are attributed to how each parameter set models atomic interactions and vibrational contributions

- The predicted specific heat values from this study align closely with available DFT-based results and previously published theoretical findings, supporting the reliability of the local harmonic approximation used in the model.

(b) coefficient of thermal expansion:

Radial and Axial CTE for BNNT and CTE for BN sheet is expressed by following expression (Guo et al.,2012)

$$\alpha_{radial}(T) = \frac{1}{\lambda_1(T)R(T)} \frac{d\left(\lambda_1(T)R(T)\right)}{dT} \tag{36a}$$

$$\alpha_{axial}(T) = \frac{1}{\lambda_2(T)r_0(T)} \frac{d\left(\lambda_2(T)r_0(T)\right)}{dT} \tag{36b}$$

$$\alpha(T) = \frac{1}{r_0(T)} \frac{d\left(r_0(T)\right)}{dT} \tag{36c}$$

The Coefficient of Thermal Expansion (CTE) quantifies how much a material expands when subjected to an increase in temperature. In the case of SWBNNTs, both the radial and axial CTEs were analysed using the multiscale framework incorporating finite temperature effects.

- At lower temperatures, the CTE values are relatively small and gradually increase, displaying a rise in curve as temperature approaches higher ranges (e.g., above 1000 K). upward trend arises due to anharmonic effects in atomic interactions becoming more pronounced at elevated temperatures.

- When comparing across different empirical parameter sets (e.g., Oh, Los, Singh), the overall trend of increasing CTE with temperature remains consistent. However, there are slight differences in the predicted values, reflecting the sensitivity of thermal behaviour to the choice of interatomic potential.

- The axial CTE values were generally smaller than the radial ones, suggesting anisotropic thermal expansion, where the tube expands more in the radial direction than along its axis. This directional dependence is due to the curvature and cylindrical structure of SWBNNTs.

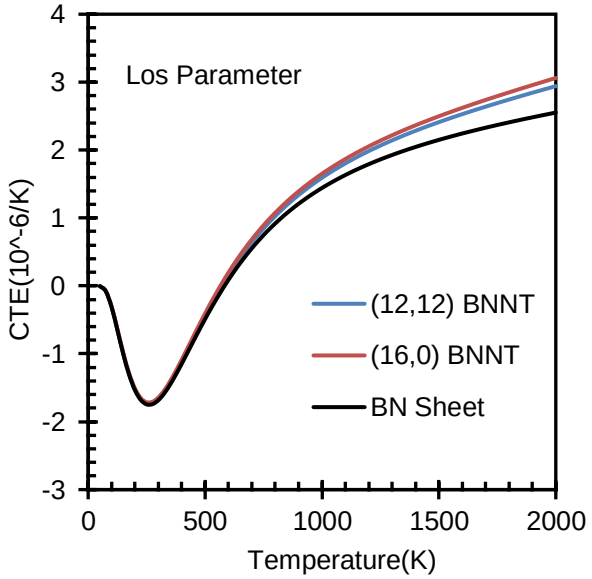

Figure 5.2. Coefficient of thermal expansion variation with temperature for BNNTs and BN sheet using Los parameter

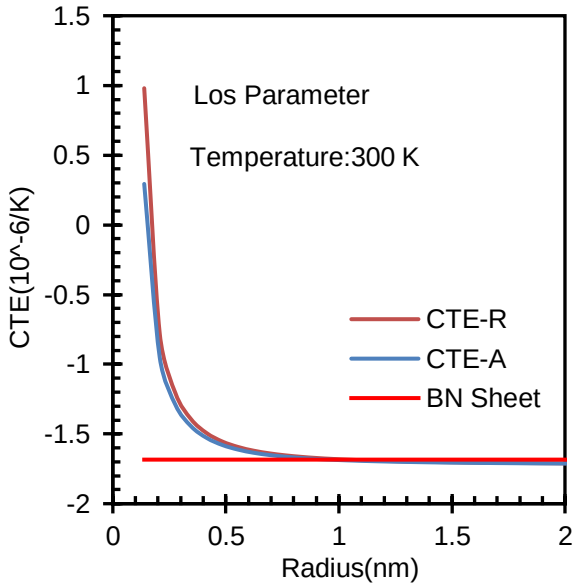

Figure 5.3. Coefficient of thermal expansion (radial and axial) of armchair BNNT with radius at 300 K temperature using Los parameter

5.1.2 Elastic properties of BNNTs:

(a) Normalized young's modulus:

To better understand how temperature affects the stiffness of SWBNNTs, the Young's modulus was normalized by its value at 0 K. This allows for a clearer comparison of stiffness reduction across a range of temperatures, regardless of the initial modulus value.

- The normalized Young's modulus decreases with rising temperature, indicating that the nanotube becomes softer as thermal energy increases. This thermal softening is due to increased atomic vibrations weakening the effective stiffness of atomic bonds.
- Across different radii, larger diameter nanotubes showed less sensitivity to temperature, meaning their normalized modulus dropped more slowly compared to smaller-radius tubes. This indicates that curvature effects amplify the impact of temperature on stiffness in smaller nanotubes.

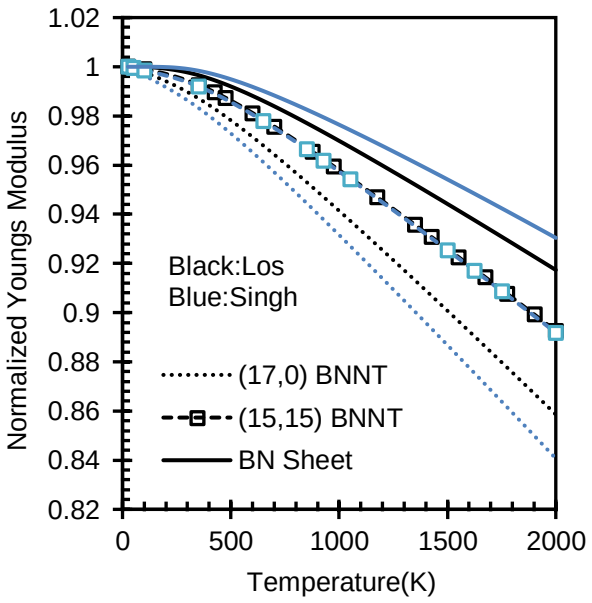

Figure 5.4. Normalized young's modulus of BNNTs and BN Sheet obtained through current finite temperature based constitutive model by using different potential parameters

(b) Youngs modulus:

The study evaluated the variation of Young's modulus of SWBNNTs as a function of radius and temperature using different sets of empirical potential parameters (Los, Singh). The simulation results demonstrated that:

Young's modulus decreases as the radius of the BNNT increases. This trend is attributed to the curvature effects becoming less significant in larger diameter nanotubes, causing their mechanical response to gradually approach that of a flat boron nitride sheet.

- The modulus values predicted by these two potential parameter sets are in close agreement with each other and align reasonably well with previously reported DFT results at 0 K, validating the accuracy of the multiscale model.

- Temperature has a softening effect on the stiffness of BNNTs, as thermal agitation reduces atomic bonding strength, thereby lowering Young's modulus.

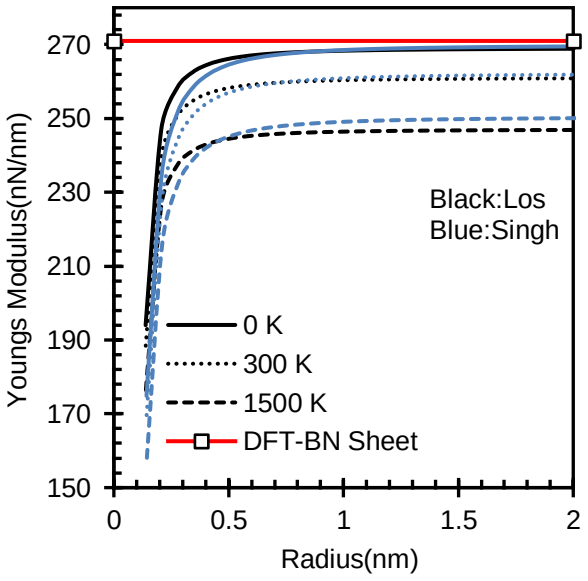

Figure 5.5. Youngs modulus variation of BNNT with radius at finite temperature by using different potential parameters and compared with BN sheet DFT results at 0 K (Kudin et al.,2001)

(c) Poisson ratio:

The Poisson's ratio, which reflects the extent of transverse contraction in response to axial stretching, also exhibited a clear dependence on radius and temperature:

- As the radius increased, a decrease in Poisson's ratio was observed. This trend reflects the diminishing curvature-induced distortion at higher radii, leading to more stable and predictable deformation behaviour.
- The predicted values were consistent with DFT reference data, reinforcing the model's capability to reproduce realistic mechanical behaviour under varying geometric conditions.
- Slight variations were noted across different parameter sets, but the overall trend remained consistent, showing reliable and robust predictions

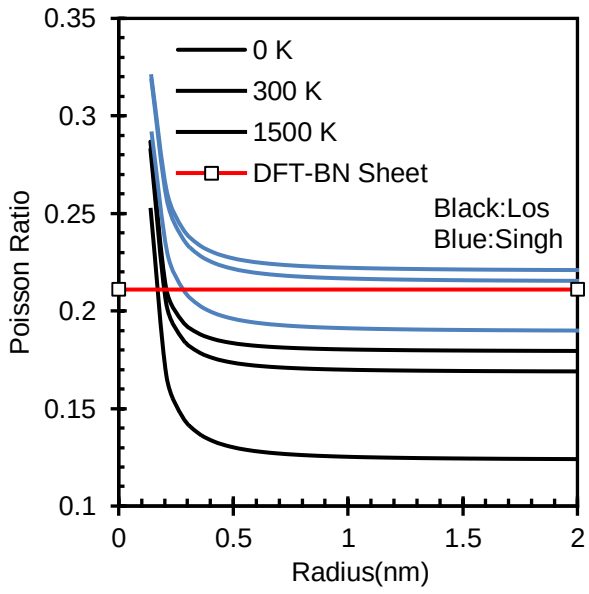

Figure 5.6. Poisson ratio variation of BNNT with radius at finite temperature by using different potential parameters and compared with BN sheet DFT results at 0 K (Kudin et al.,2001)

(d) Shear modulus:

The shear modulus characterizes the nanotube's resistance to shape deformation (shearing) and was computed from the components of the tangent stiffness matrix:

- Similar to Young's modulus, the shear modulus decreased with increasing radius, confirming the influence of curvature in smaller tubes, which enhances stiffness.
- Temperature-dependent results indicated a gradual reduction in shear modulus as temperature increased, consistent with expected thermal softening effects in nanostructured materials.
- All three parameter sets used in the model predicted comparable trends, and the results fell within the expected theoretical range derived from prior quantum and continuum studies.

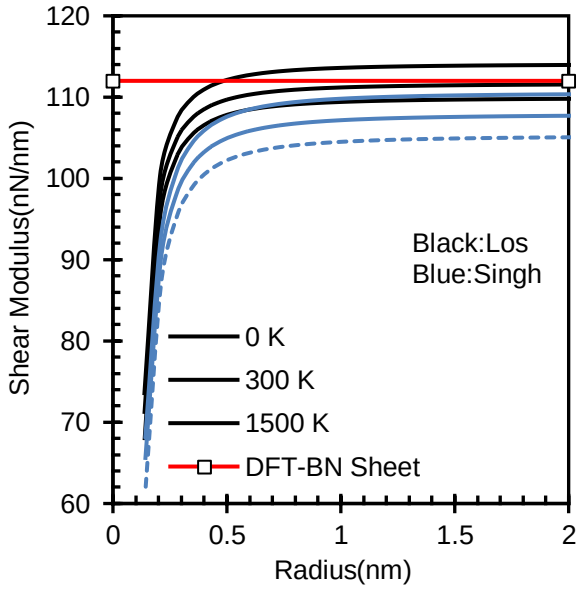

Figure 5.7. Shear modulus variation of BNNT with radius at finite temperature by using different potential parameters and compared with BN sheet DFT results at 0 K (Kudin et al.,2001)

5.1.3 Energy calculations of BNNTs:

(a) Strain energy:

Strain energy is defined as difference of the energy per atom of tube to the corresponding flat Sheet, strain energy variation with radius calculated with radius using Los and Singh parameter and compare with DFT results of (Hernandez et al., 1998) and it is in close agreement with results obtained through Singh parameter.

- The results revealed that strain energy decreases with increasing radius of the nanotube. This behaviour is expected because curvature-induced distortion is more prominent in smaller-diameter tubes, which increases the amount of energy stored under strain. As the diameter grows, the curvature effect diminishes, and the structure behaves more like a flat sheet, resulting in lower strain energy.

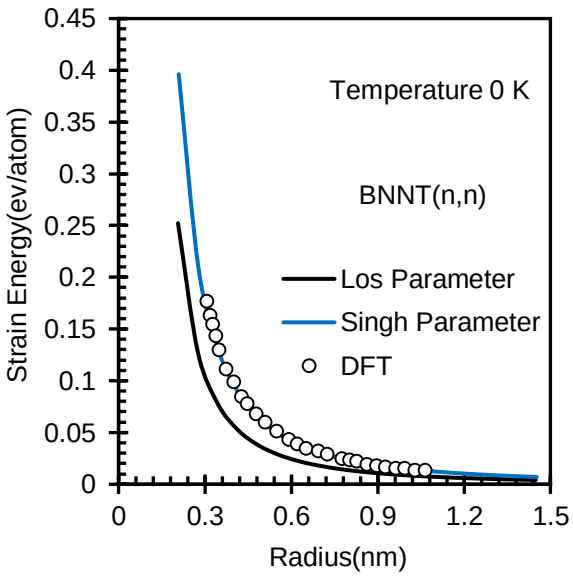

Figure 5.8. Strain energy variation of armchair BNNT with radius by using different potential parameters and compared with DFT results (Hernandez et al.,1998)

- Across all tested empirical parameter sets (Los and Singh), this decreasing trend remains consistent, though the exact numerical values

vary slightly. These variations reflect differences in how each potential captures the interatomic interactions under strain.

- Additionally, the strain energy values obtained in this study were found to be in good agreement with existing DFT data, which validates the accuracy of the multiscale modelling approach used.

(b) Cohesive energy:

Cohesive energy is a measure of the total energy required to disassemble a material into its individual atoms. It reflects the strength of the atomic bonds within the structure and serves as a key indicator of thermodynamic stability.

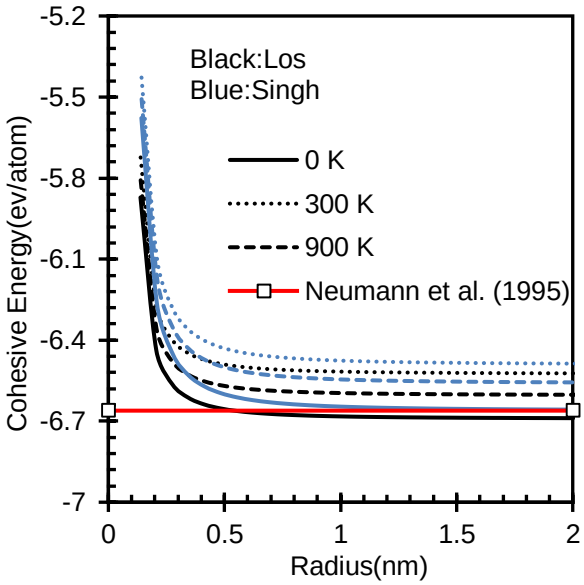

Figure 5.9. Cohesive energy variation of BNNT with radius at finite temperature by using different potential parameters and compared with results given by Neumann et al. (1995)

- The computed cohesive energy values for SWBNNTs were negative, indicating that the structure is energetically stable. The magnitude of cohesive energy increases (i.e., becomes less negative) with increasing radius. This means that smaller-radius nanotubes are more tightly bound due to higher curvature-induced stress, while larger-radius

tubes are slightly less bound, approaching the energy state of flat boron nitride sheets.

- This trend implies that as the nanotube becomes wider, its cohesive energy converges toward that of a monolayer BN sheet, where atoms experience minimal out-of-plane distortion.
- Like strain energy, cohesive energy values showed minor variations across different potential parameter sets, but the overall trend remained consistent

5.2 Free vibration analysis results of BNNTs:

5.2.1 Temperature Effect on first six modes of BNNTs:

The vibrational behavior of SWBNNTs is significantly influenced by temperature, as observed through the variation in their first six natural frequencies. These frequencies correspond to the fundamental modes of vibration that characterize how the nanotube deforms under dynamic excitation. The analysis was conducted for both (6,6), (8,8) armchair and (10,0), (14,0) zigzag nanotube configurations under clamped–clamped boundary conditions, evaluated at 300 K, 900 K, and 1500 K using the developed finite temperature-based multiscale model.

- For both armchair and zigzag SWBNNTs, a systematic decrease in the first six natural frequencies was observed as temperature increased from 300 K to 1500 K.
- This is primarily due to thermal softening, where increased atomic vibrations at higher temperatures reduce bond stiffness, resulting in a lower resistance to dynamic deformation.
- The frequency reduction is more pronounced in higher-order modes, particularly those involving radial deformation, reflecting their greater sensitivity to thermal effects.

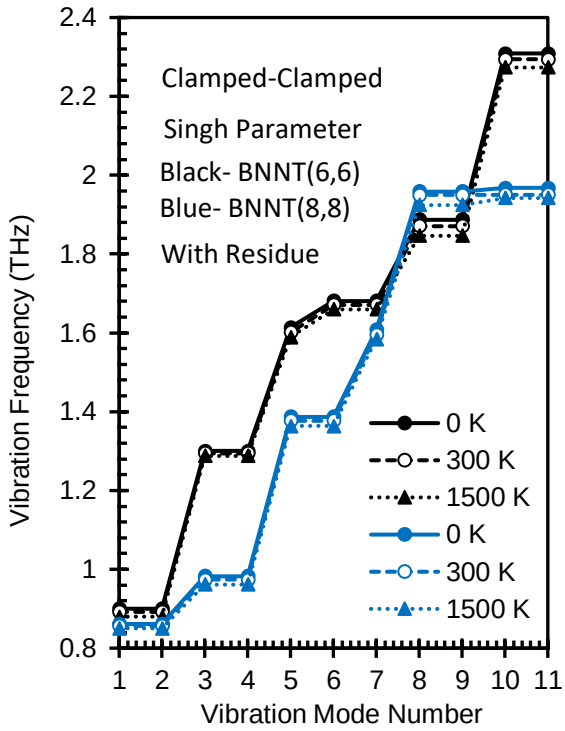

Figure 5.10. First six fundamental frequencies of armchair BNNT at finite temperature for clamped-clamped boundary conditions

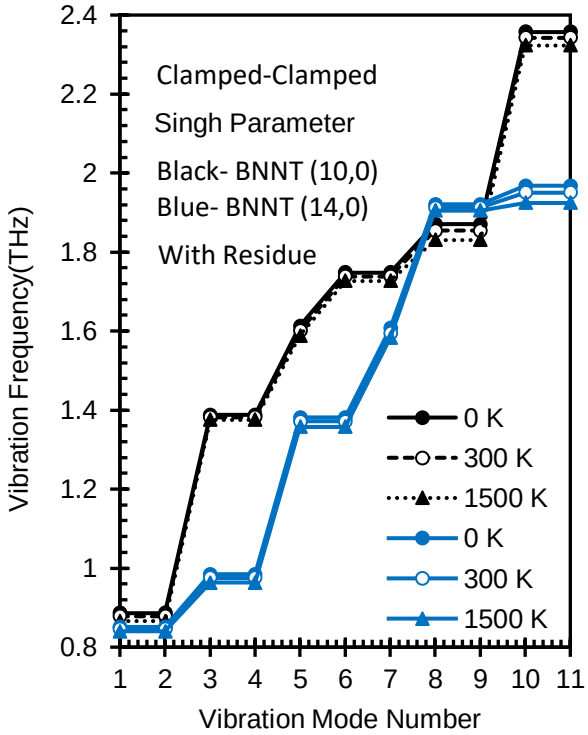

Figure 5.11. First six fundamental frequencies of zigzag BNNT at finite temperature for clamped-clamped boundary conditions

The trends obtained from this analysis closely match with available molecular dynamics (MD) simulation results at 0 K, as shown in **Figure 15** validating the accuracy of the multiscale model for capturing temperature-dependent dynamic properties.

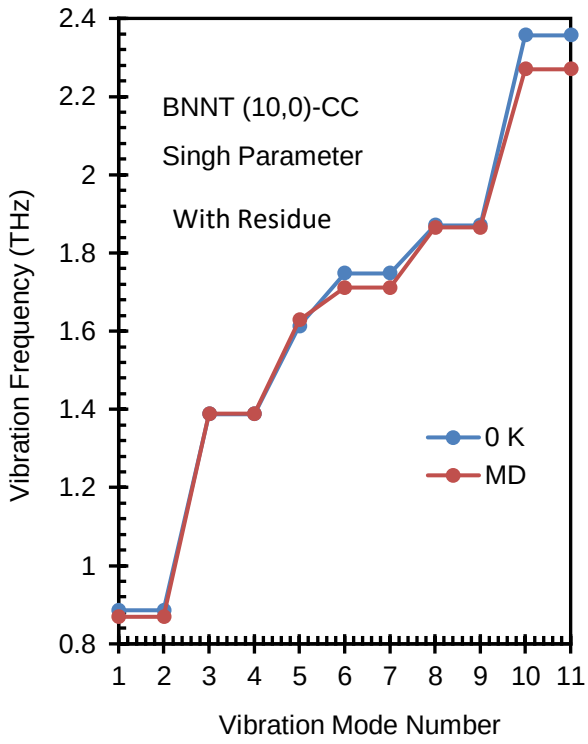

Figure 5.12. First six fundamental frequencies at 0 K for (10,0) BNNT for camped-clamped boundary conditions and results compared with MD simulation results. (Singh et al.,2023)

5.2.2 First natural frequency variation with radius at finite temperature:

This section examines how the first natural frequency of single-walled boron nitride nanotubes (SWBNNTs) varies with tube radius at finite temperature. The study is conducted using (7,7) to (16,16) armchair and (12,0) to (26,0) zigzag configurations of length 6nm. Frequencies are computed for a range of radii using the developed finite temperature-based multiscale model, and the trends are analyzed in terms of mechanical behavior and geometric dependence.

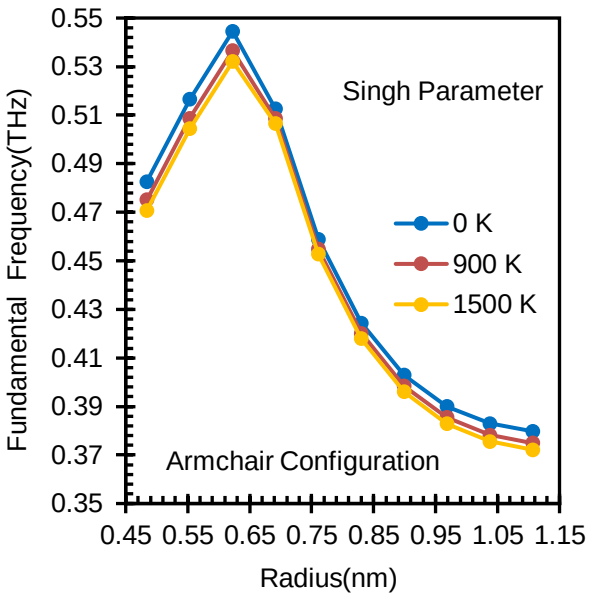

Figure 5.13. First natural frequency variation of armchair BNNT with radius at finite temperature

- With increase in radius, first natural frequency increases up to a certain radius then decreases after that, for all finite temperatures
- The critical radius exists from where trend of curve changes due to swapping of modes, up to critical radius beam bending mode will dominate and after critical radius that mode swap to shell modes due to which frequency decreases after critical radius
- At higher temperatures due to thermal softening the stiffness of the tube reduces results in decrease in first natural frequency
- Chirality effect is on natural frequency variation with radius is insignificant as size of the tube is same
- While frequency values decrease with temperature, the corresponding mode shapes remain unchanged. This indicates that the temperature affects the energy landscape but not the fundamental vibration mechanism of the nanotube.

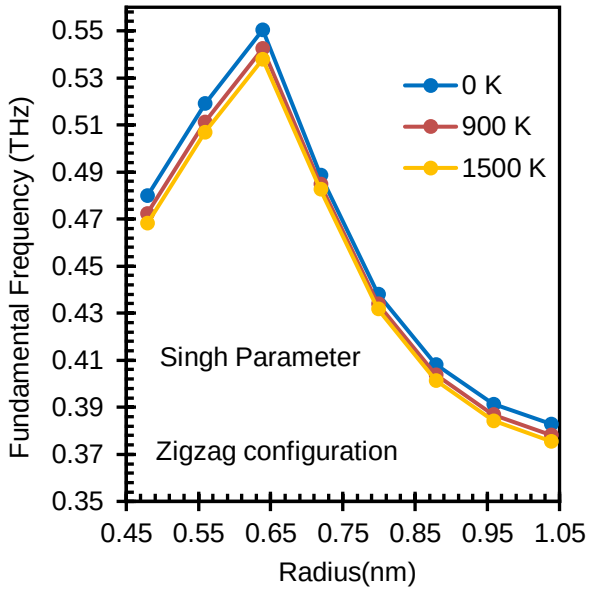

Figure 5.14. First natural frequency variation of zigzag BNNT with radius at finite temperature

The computed natural frequencies using Oh parameter show good agreement with existing theoretical data from literature (Yan et al.,2017), validating the robustness of the model.

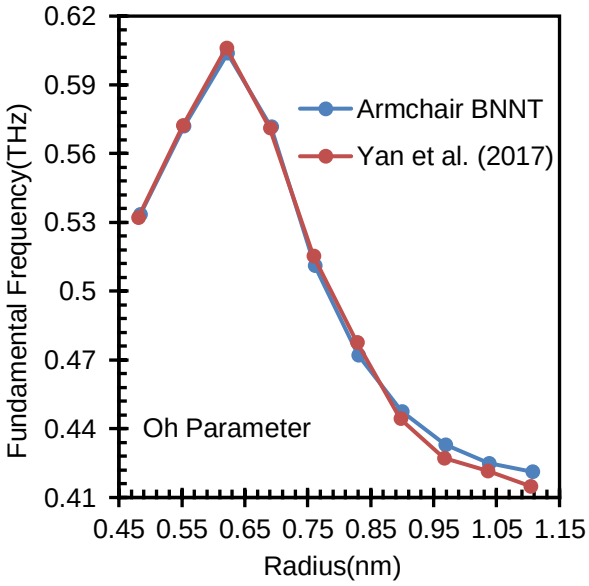

Figure 5.15. First natural frequency of variation of armchair BNNT with radius by using oh parameter and results compared with other theoretical results (Yan et al.,2017)

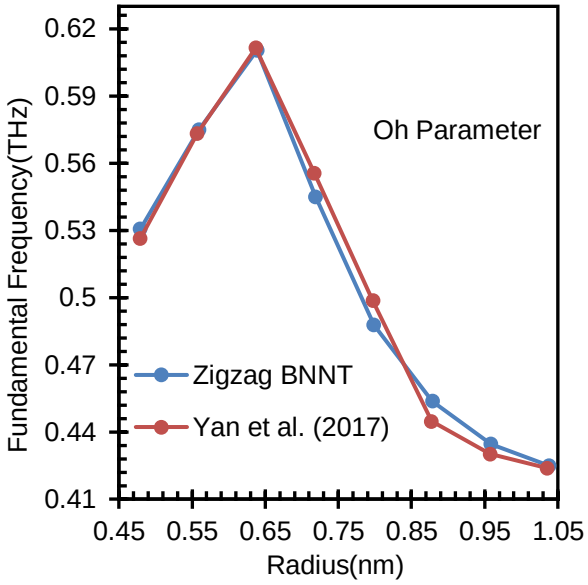

Figure 5.16. First natural frequency of variation of zigzag BNNT with radius by using oh parameter and results compared with other theoretical results (Yan et al.,2017)

5.2.3 First natural frequency variation with length at finite temperature:

This section investigates how the first natural frequency of single-walled boron nitride nanotubes (SWBNNTs) changes with variation in tube length, The analysis is carried out at a constant temperature of 300 K, using two different boundary conditions: clamped–clamped (C–C) and simply supported (S–S), for both (8,8), (10,10), (12,12) armchair and (14,0), (18,0), (21,0) zigzag configurations.

- For both chirality's and boundary conditions, the first natural frequency decreases as the length of the nanotube increases. This trend is expected, as longer tubes have lower structural stiffness in bending, leading to reduced vibrational frequencies.

- The clamped–clamped (C–C) condition consistently results in higher natural frequencies compared to the simply supported (S–S) case for lower length and greater radius. This is due to local shell modes dominates at lower length and greater radius, but at higher length and

lower radius beam modes dominates in that case boundary condition effect diminishes

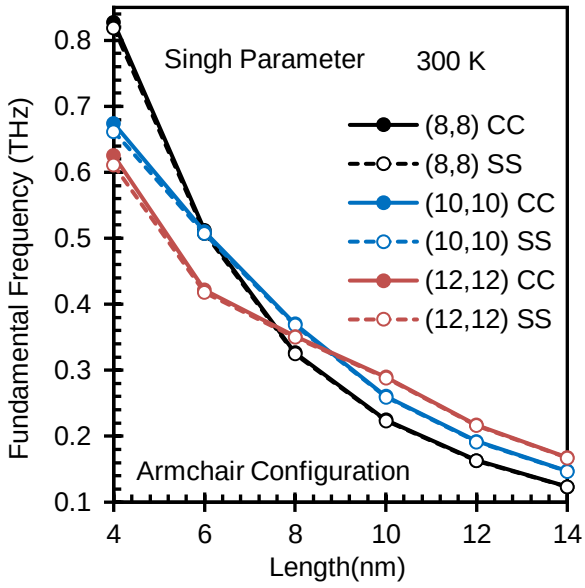

Figure 5.17. First fundamental natural variation of armchair BNNT with length at finite temperature for simply supported and clamped-clamped boundary conditions

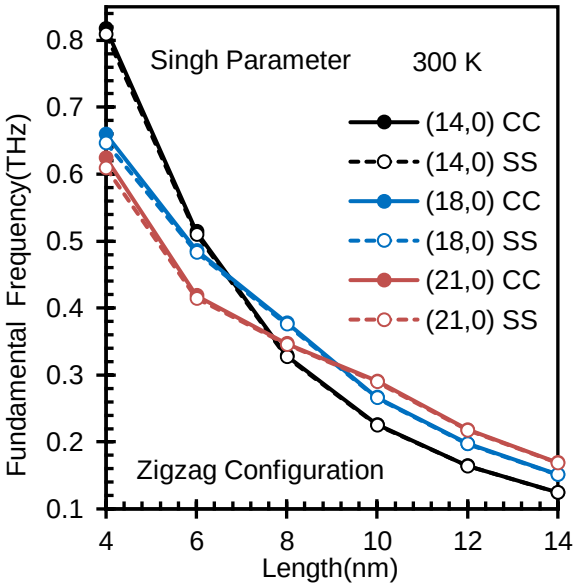

Figure 5.18. First fundamental frequency variation of zigzag BNNT with length at finite temperature for simply supported and clamped-clamped boundary conditions

- The armchair SWBNNT exhibits nearly same natural frequencies as like zigzag SWBNNT for same size and boundary condition.

5.2.4 Effect of residual strain on natural frequency at finite temperature:

Residual Strain Leads to Higher Frequencies:

- Across all modes and temperatures, the frequencies obtained with residual strain (F_W) are slightly higher than those without residual strain ($F_{W/O}$).
- This indicates that residual strain increases the effective stiffness of the nanotube, resulting in higher vibrational frequencies.
- Residual strain particularly tensile residual strain introduces an initial pre-stress in the nanotube along its axial direction. Here's why that leads to increased natural frequencies
- Percentage difference between frequencies with and without residual effect is greater for small diameter BNNT, because at low radius curvature induce more residual strain.
- While the influence of residual strain is present at all temperatures, its effect becomes slightly more pronounced at higher temperatures. This could be due to the interplay between thermal softening and mechanical pre-strain, which leads to a more balanced stiffness configuration at elevated temperatures.
- Despite the quantitative changes in frequency values, the corresponding mode shapes (as discussed later in mode shape section) remain qualitatively unchanged. This reinforces that residual strain affects the stiffness magnitude but does not induce instability or mode coupling.
- For tubes with larger radii, the relative impact of residual strain diminishes. This suggests a curvature-dependent strain energy

relaxation, where flatter geometries inherently possess lower stored energy and hence less pronounced residual effects.

- Solving residual strain improved accuracy and closer match with realistic behavior justify this inclusion in multiscale simulations.

The table shows the effect of residual strain on natural frequencies for a (3,3) BNNT, under clamped–clamped (C–C) boundary conditions, at three temperatures (300 K, 900 K, 1500 K) using the Singh (2020) potential parameters

Table 5.1. Natural frequencies of first six modes of armchair BNNT with and without residual strain at finite temperature

BNNT Configuration: BNNT (3,3); Length:3.763892nm-CC									
Parameter: Singh (2020)									
Temperature	300 K			900 K			1500 K		
Sr. No	$F_{W/O}$	F_W	% DIFF	$F_{W/O}$	F_W	% DIFF	$F_{W/O}$	F_W	% DIFF
1	0.61	0.63	1.69	0.61	0.62	1.76	0.60	0.62	1.83
2	0.61	0.63	1.69	0.61	0.62	1.76	0.60	0.62	1.83
3	1.46	1.49	1.63	1.45	1.48	1.69	1.44	1.47	1.76
4	1.46	1.49	1.63	1.45	1.48	1.69	1.44	1.47	1.76
5	1.60	1.62	1.21	1.60	1.62	1.25	1.59	1.61	1.29
6	2.49	2.53	1.80	2.47	2.52	1.88	2.44	2.49	1.97
7	2.50	2.54	1.59	2.49	2.53	1.65	2.47	2.51	1.72
8	2.50	2.54	1.59	2.49	2.53	1.65	2.47	2.51	1.72
9	3.21	3.25	1.21	3.20	3.24	1.25	3.19	3.23	1.29

The table shows the effect of residual strain on natural frequencies for a (5,0) BNNT, under clamped–clamped (C–C) boundary conditions, at three temperatures (300 K, 900 K, 1500 K) using the Singh (2020) potential. parameters

Table 5.2. Natural frequencies of first six modes of zigzag BNNT with and without residual strain at finite temperature

BNNT Configuration: BNNT (5,0); Length:3.7666nm-CC									
Parameter: Singh (2020)									
Temperature	300 K			900 K			1500 K		
Sr. No	$F_{W/O}$	F_W	% DIFF	$F_{W/O}$	F_W	% DIFF	$F_{W/O}$	F_W	% DIFF
1	0.60	0.61	2.21	0.60	0.61	2.29	0.59	0.60	2.40
2	0.60	0.61	2.21	0.60	0.61	2.29	0.59	0.60	2.40
3	1.43	1.46	2.13	1.42	1.46	2.21	1.41	1.44	2.31
4	1.43	1.46	2.13	1.42	1.46	2.21	1.41	1.44	2.31
5	1.60	1.63	1.58	1.60	1.63	1.63	1.59	1.62	1.69
6	2.46	2.51	2.08	2.45	2.50	2.16	2.43	2.48	2.25
7	2.46	2.51	2.08	2.45	2.50	2.16	2.43	2.48	2.25
8	2.49	2.55	2.35	2.47	2.53	2.45	2.44	2.50	2.56
9	3.21	3.26	1.58	3.20	3.25	1.63	3.18	3.24	1.69

5.2.5 Mode shapes of BNNTs at finite temperature:

The mode shapes of single-walled boron nitride nanotubes (SWBNNTs) reflect the deformation patterns the structure undergoes when vibrating at its natural frequencies. This study presents the first six fundamental modes for both armchair (8,8) and zigzag (10,0) configurations under clamped-clamped

boundary conditions at two distinct temperatures: 300 K and 1500 K. The aim is to understand how thermal effects influence these vibrational behaviours.

Despite significant changes in temperature, the qualitative nature of the mode shapes remains stable, despite this softening, the qualitative nature of the vibrational modes, such as axial bending, torsional, or radial modes, remains unaffected. though the associated frequencies decrease due to thermal softening. The thermal environment leads to increased atomic vibration and reduced bond stiffness, which lowers the resistance to deformation and hence the vibrational frequencies. However, this indicates that the geometric configuration and boundary constraints dominate the deformation pattern, while temperature primarily influences the dynamic response magnitude (i.e., frequency values).

These results demonstrate that the developed multiscale model accurately captures the thermally induced changes in vibrational behavior without compromising the structural integrity of the mode shape profiles. It underscores the reliability of the model in predicting vibration behavior of BNNTs in environments where thermal effects are significant, which is vital for applications in nano resonators, sensors, or thermally active nanodevices.

the structural integrity of the mode shape profiles. It underscores the reliability of the model in predicting vibration behavior of BNNTs in environments where thermal effects are significant, which is vital for applications in nano resonators, sensors, or thermally active nanodevices. The study highlights that while higher temperatures may reduce vibrational frequencies due to bond weakening, they do not cause mode switching or significant distortion of vibrational patterns. This stability is essential for the reliable design of BNNT-based nanodevices operating in extreme environments.

First six mode shapes of armchair and zigzag BNNTs at finite temperature is presented on the next page.

300 K

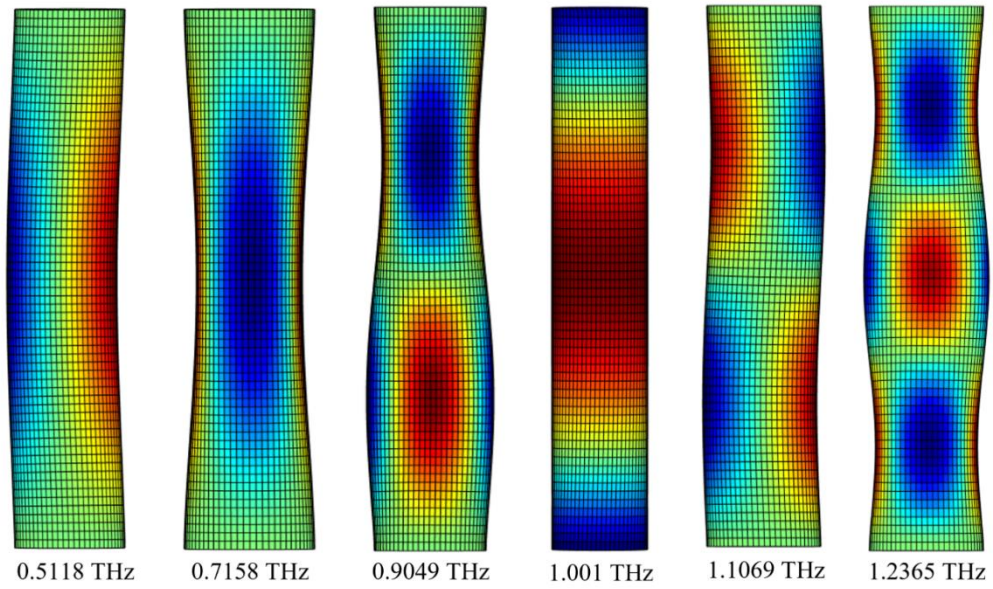

Figure 5.19. First six modes of vibration of (8,8) BNNT of Length=6nm, with clamped-clamped boundary condition at 300 K Temperature.

1500 K

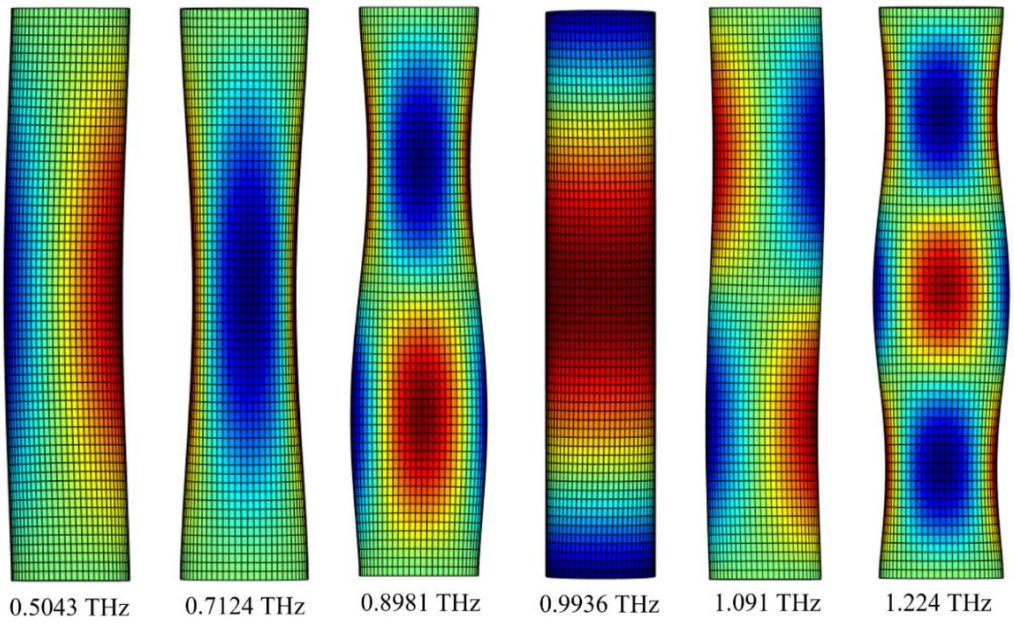

Figure 5.20. First six modes of vibration of (8,8) BNNT of Length=6nm, with clamped-clamped boundary condition at 1500 K Temperature.

300 K

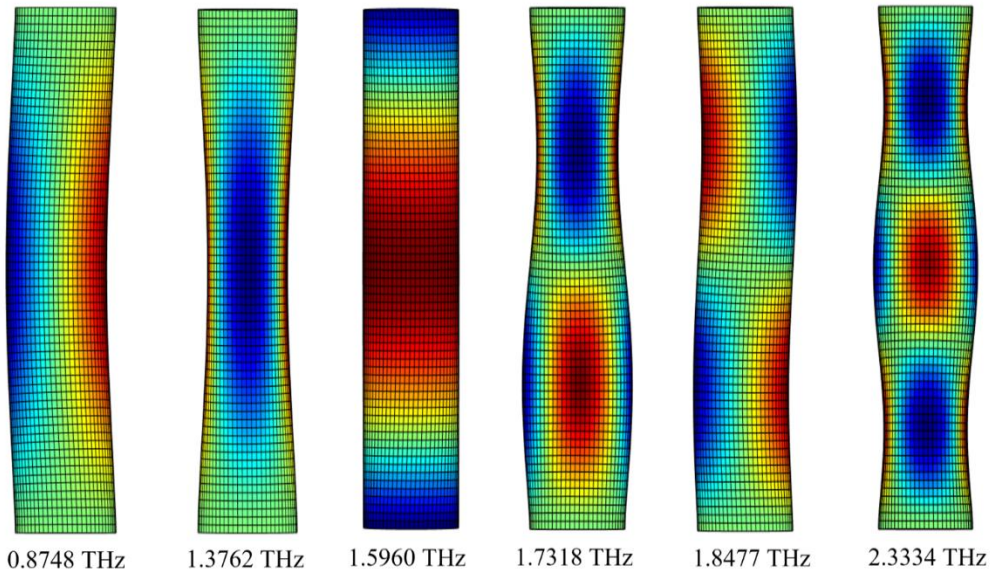

Figure 5.21. First six modes of vibration of (10,0) BNNT of Length=3.7666nm, with clamped-clamped boundary condition at 300 K Temperature.

1500 K

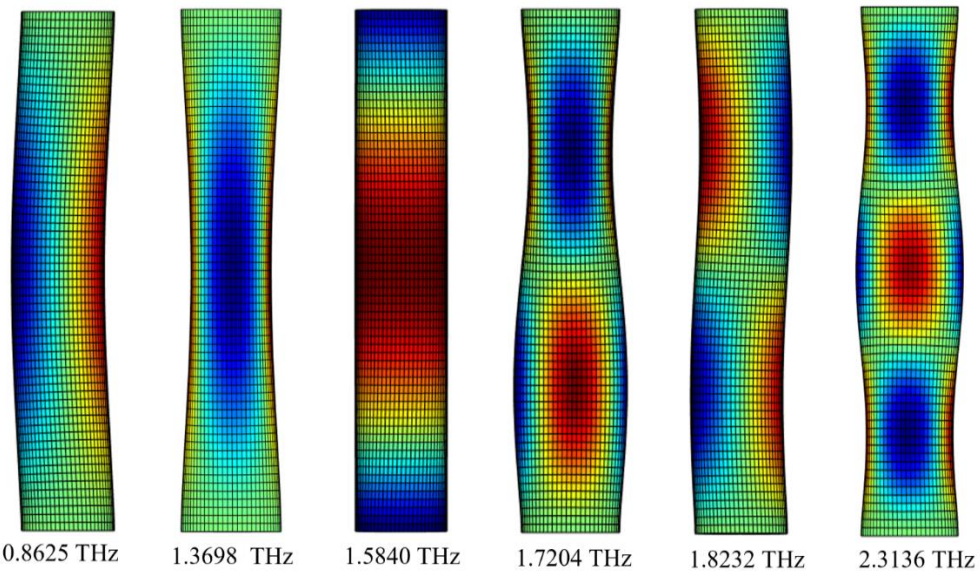

Figure 5.22. First six modes of vibration of (10,0) BNNT of Length=3.7666nm, with clamped-clamped boundary condition at 1500 K Temperature.

Chapter 6

Conclusion and Future scope

6. Introduction:

The final chapter summarizes the main findings and contributions of the research. It emphasizes the effectiveness of the multiscale modeling framework in capturing the coupled thermal-mechanical-vibrational response of SWBNNTs. The chapter also discusses potential directions for future work, including extension to multi-walled nanotubes, buckling and post-buckling analysis, dynamic and impact loading, and coupling with electrical fields for multifunctional applications. Suggestions are made to enhance computational tools and explore experimental validation.

6.1 Conclusion

The present study focused on the development and implementation of a multiscale computational framework to investigate the thermal, mechanical, and vibrational properties of single-walled boron nitride nanotubes (SWBNNTs) under finite temperature conditions. The key conclusions drawn from this research are as follows:

1. A finite temperature-based multiscale constitutive model was successfully developed using a temperature-dependent quadratic-type Cauchy-Born rule. The Tersoff–Brenner potential was incorporated with various parameter sets, and thermal vibrations were captured through the local harmonic approximation (LHA), providing a realistic representation of atomic interactions at elevated temperatures.

2. Thermal properties such as specific heat and coefficient of thermal expansion (CTE) were evaluated. The predicted results showed good agreement with available DFT data. Specific heat showed asymptotic behaviour beyond 1500 K, while both radial and axial CTE varied consistently with radius and temperature.

3. Elastic properties including Young's modulus, Poisson's ratio, and shear modulus were extracted from the tangent stiffness matrix. These properties were found to be sensitive to temperature and radius, with the modulus values approaching those of flat BN sheets as radius increased.

4. Free vibration characteristics were evaluated through a finite element framework incorporating a four-nodded membrane-consistent element. This approach effectively captured free vibration characteristics while avoiding membrane locking.

5. Modal analysis results showed that the first six vibration modes account for approximately 80.62% of the total modal mass participation, confirming that these modes are dominant in the dynamic response of SWBNNTs. Higher modes contribute less than 5% each and were excluded to ensure computational efficiency without compromising accuracy.

6. The influence of temperature, radius, and length on the natural frequencies of SWBNNTs was studied under various boundary conditions. Increasing temperature was observed to reduce natural frequencies, while both radius and length variations significantly altered vibrational responses.

7. Mode shape evolution across temperature ranges revealed that fundamental vibration patterns are preserved at elevated temperatures, although the frequency values shift due to thermal softening effects.

6.2 Future Scope

While this research establishes a strong foundation for modelling and analysing SWBNNTs at finite temperatures, several avenues remain open for future exploration:

- Extension to multi-walled BNNTs: The current work focuses on single-walled structures. Investigating multi-walled BNNTs could provide insights into interlayer interactions, which are critical for real-world applications where such structures are more common.
- Dynamic and impact loading: Future studies may include the analysis of time-dependent and impact-based load conditions to understand the response of BNNTs in real-time dynamic applications such as sensors, actuators, or aerospace components.
- Extension of the developed framework to analyze buckling behavior and nonlinear static response of SWBNNTs under combined thermal and mechanical loading would provide deeper insights into stability limits and post-buckling deformation patterns, especially for large deformation regimes and complex boundary conditions.
- Thermo-electromechanical coupling: A promising extension would be to integrate electrical properties into the model, enabling the study of BNNTs in multifunctional devices subjected to coupled thermal and electrical fields.

REFERENCES

1. Chopra, N. G., Luyken, R. J., Cherrey, K., Crespi, V. H., Cohen, M. L., Louie, S. G., & Zettl, A. (1995). Boron nitride nanotubes. *science*, *269*(5226), 966-967.
2. Krishnan, A., Dujardin, E., Ebbesen, T. W., Yianilos, P. N., & Treacy, M. M. (1998). Young's modulus of single-walled nanotubes. *Physical review B*, *58*(20), 14013.
3. Rafiee, R., & Moghadam, R. M. (2014). On the modeling of carbon nanotubes: a critical review. *Composites Part B: Engineering*, *56*, 435-449.
4. Yoon, J., Ru, C. Q., & Mioduchowski, A. (2003). Vibration of an embedded multiwall carbon nanotube. *Composites Science and Technology*, *63*(11), 1533-1542.
5. Zhang, Y., Liu, G., & Han, X. (2005). Transverse vibrations of double-walled carbon nanotubes under compressive axial load. *Physics Letters A*, *340*(1-4), 258-266.
6. Natsuki, T., Lei, X. W., Ni, Q. Q., & Endo, M. (2010). Vibrational analysis of double-walled carbon nanotubes with inner and outer nanotubes of different lengths. *Physics Letters A*, *374*(46), 4684-4689.
7. Wang, Q., & Varadan, V. K. (2006). Vibration of carbon nanotubes studied using nonlocal continuum mechanics. *Smart materials and structures*, *15*(2), 659.
8. Hernandez, E., Goze, C., Bernier, P., & Rubio, A. (1998). Elastic properties of C and B x C y N z composite nanotubes. *Physical Review Letters*, *80*(20), 4502.
9. Kudin, K. N., Scuseria, G. E., & Yakobson, B. I. (2001). C 2 F, BN, and C nanoshell elasticity from ab initio computations. *Physical Review B*, *64*(23), 235406.

10. Han, T., Luo, Y., & Wang, C. (2013). Effects of temperature and strain rate on the mechanical properties of hexagonal boron nitride nanosheets. *Journal of Physics D: Applied Physics*, *47*(2), 025303.
11. Gao, W., & Huang, R. (2014). Thermomechanics of monolayer graphene: Rippling, thermal expansion and elasticity. *Journal of the Mechanics and Physics of Solids*, *66*, 42-58.
12. Guo, X., Wang, J. B., & Zhang, H. (2006). Mechanical properties of single-walled carbon nanotubes based on higher order Cauchy–Born rule. *International Journal of Solids and Structures*, *43*(5), 1276-1290.
13. Wang, J. B., Guo, X., Zhang, H. W., Wang, L., & Liao, J. (2006). Energy and mechanical properties of single-walled carbon nanotubes predicted using the higher order Cauchy-Born rule. *Physical Review B—Condensed Matter and Materials Physics, 73*(11), 115428.
14. Huang, Y., Wu, J., & Hwang, K. C. (2006). Thickness of graphene and single-wall carbon nanotubes. *Physical Review B—Condensed Matter and Materials Physics*, *74*(24), 245413.
15. Arroyo, M., & Belytschko, T. (2002). An atomistic-based finite deformation membrane for single layer crystalline films. *Journal of the Mechanics and Physics of Solids*, *50*(9), 1941-1977.
16. Arroyo, M., & Belytschko, T. (2004). Finite crystal elasticity of carbon nanotubes based on the exponential Cauchy-Born rule. *Physical Review B*, *69*(11), 115415.
17. Yan, J. W., & Liew, K. M. (2015). Predicting elastic properties of single-walled boron nitride nanotubes and nanocones using an atomistic-continuum approach. *Composite Structures*, *125*, 489-498.
18. Jiang, H., Huang, Y., & Hwang, K. C. (2005). A finite-temperature continuum theory based on interatomic potentials.
19. Guo, X., Liao, J., & Wang, X. (2012). Investigation of the thermo-mechanical properties of single-walled carbon nanotubes based on

the temperature-related higher order Cauchy–Born rule. *Computational materials science*, *51*(1), 445-454.

20. Raikwar, A., & Singh, S. (2024). Elastic properties and constitutive behaviour of graphene at finite temperature and large deformation. *European Journal of Mechanics-A/Solids*, *105*, 105247.
21. Singh, S. (2020). Critical assessment of the interatomic potentials for the elastic properties of the noncarbon monolayer nanomaterials. *Computational Materials Science*, *177*, 109550.
22. Singh, S., Ravi Raj, B. M., Mali, K. D., & Watts, G. (2021). Elastic properties and nonlinear elasticity of the noncarbon hexagonal lattice nanomaterials based on the multiscale modeling. *Journal of Engineering Materials and Technology*, *143*(2), 021006.
23. Kitipornchai, S., He, X. Q., & Liew, K. M. (2005). Continuum model for the vibration of multilayered graphene sheets. *Physical Review B—Condensed Matter and Materials Physics*, *72*(7), 075443.
24. Rouhi, S., & Ansari, R. (2012). Atomistic finite element model for axial buckling and vibration analysis of single-layered graphene sheets. *Physica E: Low-dimensional Systems and Nanostructures*, *44*(4), 764-772.
25. Arghavan, S., & Singh, A. V. (2011). Free vibration of single layer graphene sheets: lattice structure versus continuum plate theories.
26. Giannopoulos, G. I., Kontoni, D. P. N., & Georgantzinos, S. K. (2016). Efficient FEM simulation of static and free vibration behavior of single walled boron nitride nanotubes. *Superlattices and Microstructures*, *96*, 111-120.
27. Panchal, M. B., Upadhyay, S. H., & Harsha, S. P. (2012). Vibration analysis of single walled boron nitride nanotube based nanoresonators. *Journal of nanotechnology in engineering and medicine*, *3*(3), 031004.
28. Wang, L., Hu, H., & Guo, W. (2010). Thermal vibration of carbon nanotubes predicted by beam models and molecular

dynamics. *Proceedings of the Royal Society A: Mathematical, Physical and Engineering Sciences*, *466*(2120), 2325-2340.

29. Chowdhury, R., Wang, C. Y., Adhikari, S., & Scarpa, F. (2010). Vibration and symmetry-breaking of boron nitride nanotubes. *Nanotechnology*, *21*(36), 365702.
30. Ansari, R., & Ajori, S. (2014). Molecular dynamics study of the torsional vibration characteristics of boron-nitride nanotubes. *Physics Letters A*, *378*(38-39), 2876-2880.
31. Ansari, R., and S. Ajori. "A molecular dynamics study on the vibration of carbon and boron nitride double-walled hybrid nanotubes." *Applied Physics A* 120 (2015): 1399-1406.
32. Darvishi, F., Rahmani, O., Ostadrahimi, A., Choi, E., & Li, G. (2024). Molecular dynamics simulation of free transverse vibration behavior of single-walled coiled carbon nanotubes. *Mechanics of Advanced Materials and Structures*, *31*(20), 5028-5039.
33. Sun, Y., & Liew, K. M. (2008). Mesh-free simulation of single-walled carbon nanotubes using higher order Cauchy–Born rule. *Computational materials science*, *42*(3), 444-452.
34. Sun, Y., & Liew, K. (2008). The buckling of single-walled carbon nanotubes upon bending: the higher order gradient continuum and mesh-free method. *Computer Methods in Applied Mechanics and Engineering*, *197*(33-40), 3001-3013.
35. Yan, J. W., Liew, K. M., & He, L. H. (2013). Free vibration analysis of single-walled carbon nanotubes using a higher-order gradient theory. *Journal of Sound and Vibration*, *332*(15), 3740-3755.
36. Yan, J. W., Zhang, L. W., Liew, K. M., & He, L. H. (2014). A higher-order gradient theory for modeling of the vibration behavior of single-wall carbon nanocones. *Applied Mathematical Modelling*, *38*(11-12), 2946-2960.
37. Yan, J. W., Tong, L. H., & Xiang, P. (2017). Free vibration analysis of single-walled boron nitride nanotubes based on a computational

mechanics framework. *Superlattices and Microstructures*, *112*, 230-248.

38. Singh, S., & Patel, B. P. (2018). Large deformation static and dynamic response of carbon nanotubes by mixed atomistic and continuum models. *International Journal of Mechanical Sciences*, *135*, 565-581.
39. Singh, S., Raj, B. R., Mali, K. D., & Joshi, R. (2023). Static analysis and vibration characteristics of some noncarbon nanotubes through atomistic continuum coupled modelling. *Archive of Applied Mechanics*, *93*(6), 2331-2350.
40. Qi, H., & Wang, X. (2023). A Multi-Scale Continuum Study for Boron Nitride Nanotubes Based on the Meshless Local Petrov–Galerkin Method. *Mechanics of Solids*, *58*(3), 994-1005.
41. Neumann, H., & Edgar, H. (1995). „Properties of Group III Nitrides.(EMIS Datareviews Series No. 11).“. *Crys. Res. Technol*, 910.
42. Los, J. H., Kroes, J. M. H., Albe, K., Gordillo, R. M., Katsnelson, M. I., & Fasolino, A. (2017). Extended Tersoff potential for boron nitride: Energetics and elastic properties of pristine and defective h-BN. *Physical Review B*, *96*(18), 184108.
43. Oh, E. S. (2010). Elastic properties of boron-nitride nanotubes through the continuum lattice approach. *Materials Letters*, *64*(7), 859-862.